NURETH14-637

EXPERIMENTAL AND THEORETICAL TOOLS TO SUPPORT THE DEVELOPMENT OF HIGH-PERFORMANCE LWR FUEL ELEMENTS

H.-M. Prasser

Swiss Federal Institute of Technology Zurich, Switzerland Paul Scherrer Institute, Villigen, Switzerland

Abstract

The fluid-dynamic optimization of fuel elements for light water reactors requires advanced CFD models and experiments with sufficiently high-resolution instrumentation. An overview is given on novel developments in this field at the ETH Zurich and the Paul Scherrer Institute. Instrumentation is based on wire-mesh sensor technology and neutron tomography, which are used in adiabatic tests. Theoretical approaches pursued are liquid film models for boiling water reactor conditions based on RANS simulations of the vapor flow, coupled with a simplified mass transport model for the liquid phase and single-phase LES to predict turbulent coolant exchange between neighboring subchannels. LES coupled with surface tracking techniques is on the way towards fundamental modeling of flow boiling, together with solving conjugate heat transfer. Existing tomography with cold neutrons is complemented by exploring the possibilities of imaging with fast neutrons.

Introduction

Worldwide, significant efforts are made to optimize the thermal performance of fuel rod bundles for light water reactors. The main goals are the enhancement of heat transfer, the delay of heat transfer crisis, both concerning DNB and dryout, the enhancement of coolant exchange between sub-channels and a reduction of pressure drop. The main degree of freedom consists in varying the geometry of functional spacer grids. Beyond their function to keep fuel rods in position, they are nowadays equipped with elements for the flow control, like vanes creating swirl and generating turbulence in the coolant, as well as intensifying cross-mixing. An additional point of interest is given by intention to reduce the moderator-to-fuel ratio, which is the major key for enhancing the fuel efficiency by hardening the neutron spectrum. After a period of considerable efforts to develop a dense lattice PWR in the nineties, the issue has recently received renewed interest with a focus shifted towards boiling water reactors. The demonstration of the reliable heat removal during normal operation and accidents is a major concern when aiming at the development of high-conversion LWRs.

One of the most important tools for experimental studies in the field is fluid dynamic instrumentation with a resolution sufficiently high to be applicable to resolve flow fields, mixing processes and gasliquid interfaces in the narrow space between the fuel rods and in the vicinity of spacer grids. Progress of two general technological lines is reported in the paper. (1) the use of wire-mesh sensors and sensor configurations based on the same signal acquisition technique, but using different electrode arrangements, and (2) recent results as well as future plans in applying neutron tomography to fuel rod studies.

For the time being, our own experiments were performed only in test rigs operated at ambient temperatures and close to atmospheric pressure. The first test rig that will be introduced is a cold

adiabatic model of a matrix of 4 x 4 sub-channels. The novelty consists in the implementation of a wire-mesh sensor into the lattice of fuel rod models. The test was used to study the cross-mixing between sub-channels in single-phase and two-phase flow conditions as well as the structure of the gas-liquid interface in case of a bubbly flow. Spacer studies are planned focusing on the effect on the cross-mixing and the interfacial structures.

The second experiment focuses on annular flow found in the top region of fuel elements for boiling water reactors. The test section represents a pair of neighboring sub-channels, which is sufficient for most of the tests needed to perform spacer grid optimization. In combination with a liquid film sensor based on the signal acquisition method of mesh sensors, the described experimental technique represents a powerful tool not only for fundamental studies, but also for spacer optimization. A special feature of this loop driving the test section is the possibility to use different gases as model fluids substituting the vapor in the real reactor. In this way, the influence of the gaseous phase can be studied, which is of particular interest at high void fractions. The loop installed at ETH Zurich can be operated with air, helium and octafluorocyclobutane (C_4F_8). In this way, the gas density can be changed by a factor of 50, whereas the density C_4F_8 is only a factor of 4 lower than the density of vapor under typical boiling water reactor conditions. In first studies on bubbly flows in narrow channels, the introduced novel sensors are used to quantify the remaining liquid film thickness underneath a bubble confined between two opposite walls.

Finally, tomography with cold neutrons was applied to a channel of identical geometry, which was used to validate the results of the electrical liquid film sensor. It turned out, that neutron tomography is a powerful complement, because liquid holdup can be characterized not only on the surface of the instrumented fuel rod, but also in the bulk of the gas flow and on the spacer structures. Furthermore, the spatial resolution of the obtained time-averaged film thickness profiles is much higher, while the electrical film sensor delivers time resolved data.

In the theoretical field, three particular own modeling efforts are presented: (1) Large Eddy Modeling (LES) used to predict cross-mixing under single phase conditions, (2) the coupling of LES with advanced surface tracking techniques aiming at the modeling of adiabatic and non-adiabatic two-phase flow, and (3) the development of a simplified model for the time averaged liquid film thickness on the surface of a fuel rod of a boiling water reactor under annular flow conditions, which includes the prediction of the spacer effect.

1. Instrumentation

1.1 Mesh sensors

1.1.1 General function

Wire-mesh sensors range back to an invention of Johnson in 1987 [1], who proposed to stretch two perpendicular grids of electrode wires across a pipe cross-section. By counting the number of crossing points which are immersed into the conducting liquid phase, it was proposed to measure the liquid holdup. The detection of the conducting phase was performed by sensing an electrical contact between a transmitter and a receiver wire. The system has not found broad application, probably because of an unreliable liquid detection due to vagabonding parasitic currents causing false detections. It was never applied for imaging.

The first imaging was performed by the group of Mewes in Hannover [2]. Three grids of parallel wires were placed into the flow. A conductivity meter was connected to each pair of adjacent parallel wires in a successive order. This was carried out by a digitally controlled multiplex unit. The effective conductance distributions measured represent a projection of the volumetric liquid fraction in the direction of the wires of the given grid. Three linearly independent projections are acquired in this way, and the phase distribution inside the measuring cross-section has to be obtained using tomographic image reconstruction techniques. As the result, an imaging frequency of about 100 Hz was reached. The fact that only three projections are available causes difficulties during the reconstruction, since the reconstruction of the image requires the solution of a strongly underdetermined inverse task in case of so few projections.

Improving quality and speed of imaging was the intention of our own development carried out at the Research Center in Rossendorf near Dresden [3]. We went back to wire-mesh sensors consisting of two planes of wire grids placed into the flow in a short distance from each other. The wires of the first plane (transmitter plane) are supplied with pulses of a driving voltage in successive order. The electrical current arriving at the transmitter wires of the second plane (receiver plane), is a measure of the average conductivity from the region between the crossing points.

The signal acquisition system (Figure 1) keeps low impedance of transmitter driver and receiver preamplifier cascades, which guarantees that the potential at all non-activated transmitter electrodes and all receiver electrodes remains always very close to ground potential. This is an important feature to suppress cross-talk.

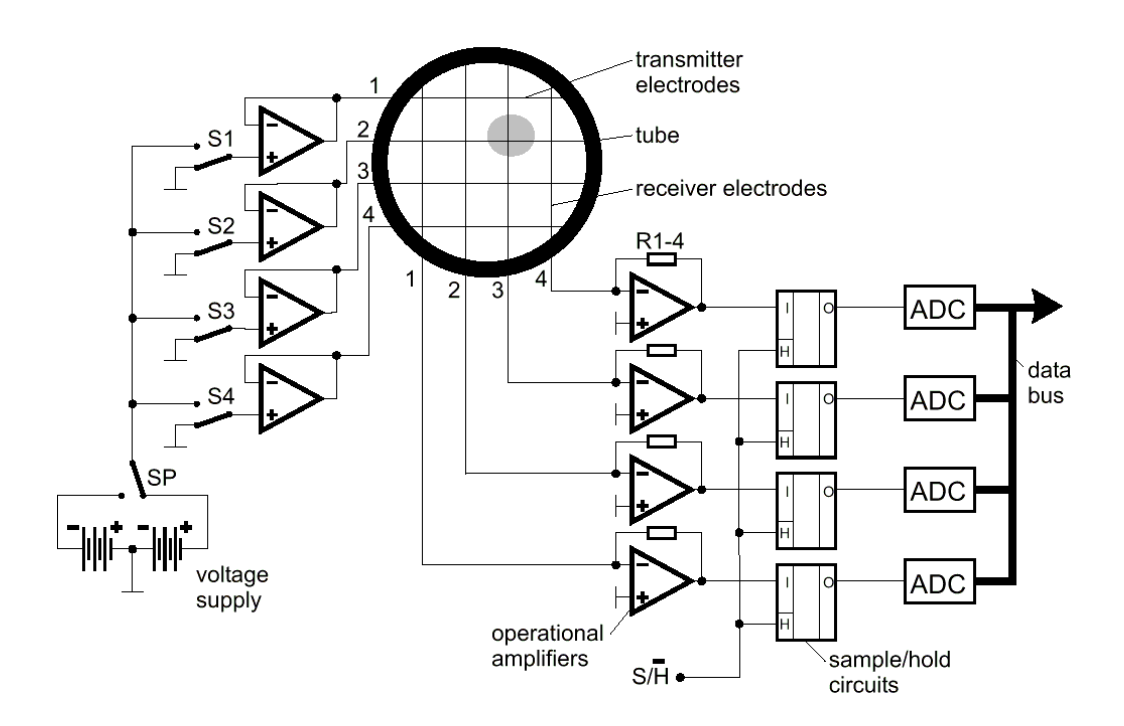


Figure 1 Simplified scheme of the signal acquisition system of a wire-mesh sensor [3]

As it will be shown below, the signal acquisition system can be used for a fast readout of the conductance of any two-dimensional matrix of individual resistive elements, independently if the individual measuring point is represented by a pair of electrodes immersed into an electrically conducting fluid, or if it is any other kind of solid-state resistor.

The signal acquisition units available as a result of a co-operation between the Research Center in Dresden/Rossendorf and TELETRONIC Ltd. are capable in reading the values from a matrix of 128 x 128 crossing points with a sampling rate of 1.25 kHz [4]. The measuring frequency depends on the size of the sensor matrix. It is inverse proportional to the number of transmitter electrodes.

1.1.2 <u>Wire-Mesh Sensors spanning over the flow cross-section</u>

The classical application of the mesh sensor technique consists in the acquisition of conductivity distributions in a measuring plane that spans over the cross-section of the flow duct [3]. Two-phase flow experiments at the TOPFLOW facility in Rossendorf may serve as examples for the detection of the gaseous phase in a liquid continuum [5-7]. Sensors were developed and applied even for high-pressure experiments up to 65 bar and 280 °C [8]. Single-phase mixing experiments using salt tracers were performed at the ROCOM test facility in Rossendorf, which is a model of a pressurized water reactor in the linear scale of 1:5 [9]. An application in a T-junction is reported in [10].

1.1.3 Wire-Mesh Sensors with electrodes on opposite walls

As an alternative to wires as electrode, they can be put on opposite walls of a duct. This is a viable solution especially for ducts with cross-sections that have a high aspect ratio, e.g. a flat rectangular channel. The electrodes are then preferably put to the pair of inner walls that are close to each other. Some freedom exists concerning the geometry of the channel. At the ROCOM test facility in Rossendorf, this kind of sensor was mounted in the downcomer of the reactor model [11, 12].

1.1.4 <u>Liquid film sensors</u>

A second type of non-intrusive sensor is the liquid film sensor used for a fast acquisition of time sequences of two-dimensional film thickness distributions [13]. It consists of an array of electrode pairs mounted flush to the wall. Transmitter electrodes form the lines (x) in this matrix shown in Figure 2, while the receiver electrodes form the columns (y).

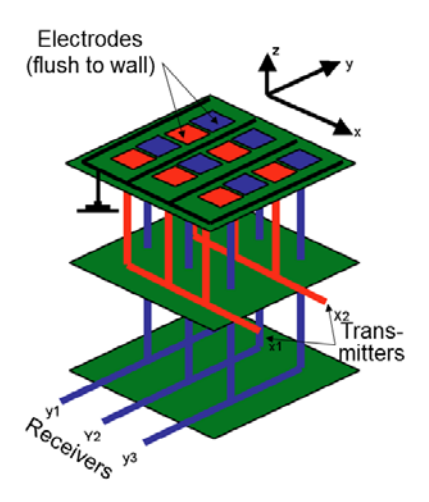


Figure 2 Basic scheme of a liquid film sensor

In this way, the signal acquisition results in a two-dimensional distribution of conductance values distributed over a domain given by the sensor surface. This arrangement of electrodes can be connected to a mesh sensor signal acquisition system. With signal acquisition units available today, a matrix of 16

x 128 measuring positions can be read out with a frequency of 10 kHz. The sensors used in fuel rod experiments will be presented in detail in section 4.2.

1.2 Neutron tomography

Thermal and cold neutrons are recognized as ideal type of radiation for detecting small amounts of light elements, above all hydrogen, in objects containing large amounts of heavy elements, like iron and steel alloying elements or others [14]. The contrast is in such a case much better that an imaging with photons (gamma radiation, X-rays), because the attenuation of photons grows with the atomic number, while neutron beams are strongly attenuated by the elastic scattering process on hydrogen, and much less by most of the heavy elements (Figure 3), of course with some exceptions of those nuclides with a high absorption cross-section, like boron, cadmium or gadolinium, which, on the other hand, can be successfully applied as tracer particles. Sometimes, as for example in molten heavy metals, benefit is taken simply from the fact that neutron radiation is not completely extinct, which would be the case for photons at the same dimensions of the object. An application of neutrons to a two-phase flow with led-bismuth eutectic as liquid is given in [15, 16]. There, the high absorption of AuCd₃ particles are used a seeds to measure velocities by a particle tracking technique.

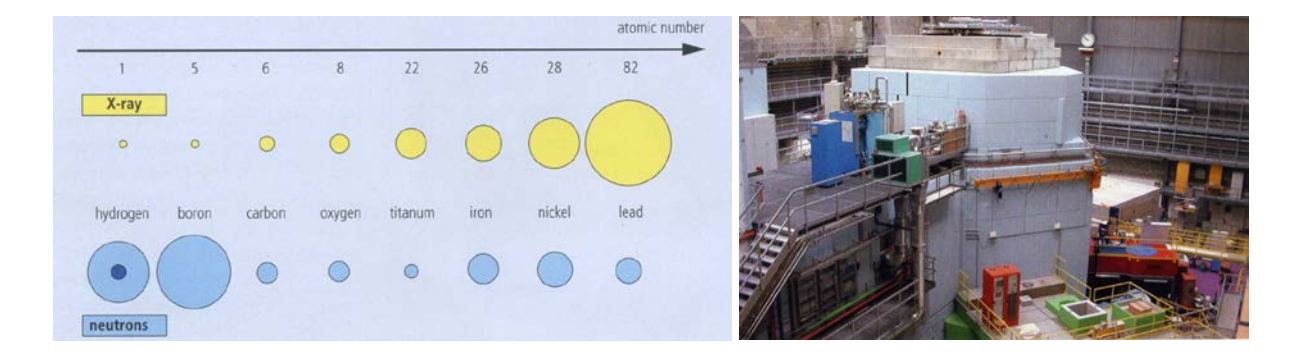


Figure 3 Attenuation of a thermal neutron beam by different elements and view of the spallation neutron source SINO (source: PSI [17])

Tomography with thermal and cold neutrons is available at two beam lines (ICON, NEUTRA) of the spallation neutron source SINQ of the Paul Scherrer Institute [17]. The cold neutrons are generated by moderation of the spallation neutrons in a tank of liquid deuterium. The beam lines and the imaging technique are described in [18, 19].

Tomography requires the acquisition of a large number of projections of the attenuation in the object under different view angles. With other words, tomography is based on a radiographic imaging that has to be repeated after a stepwise rotation of either the tomography setup around the object or a rotation of the object under the beam. Strong neutron sources are mighty machines - research reactors or, as in case of the PSI, spallation sources coupled with a large proton accelerator. Therefore, the only possible way is the rotation of the object.

In the present paper, an application of cold neutron tomography to a model representing a pair of neighboring sub-channels of a fuel element for boiling water reactors is described. Although neutron tomography is still a quite new approach in the field of multiphase flows, there are several publications showing an increasing interest in this technique. Using neutron radiography/tomography for fuel

bundle research, Takenaka et al. have performed a number of studies [20, 21] and compared the performance of fast and thermal neutron imaging [22]. Lim et al. [23] performed high-frame rate thermal neutron radiography on a model fuel bundle. Along this line, the pioneering research by Kureta et al. [24-26] must be also mentioned who have performed comprehensive investigations on tight-lattice heated fuel bundles of an advanced BWR design using thermal neutron tomography. They examined different flow regimes including annular flow but did not go so far as to characterize liquid film thickness distributions on the pins.

2. Single-phase cross-mixing in fuel rod bundles

2.1 Cold Adiabatic Experiments in a Model representing 4 x 4 sub-channels

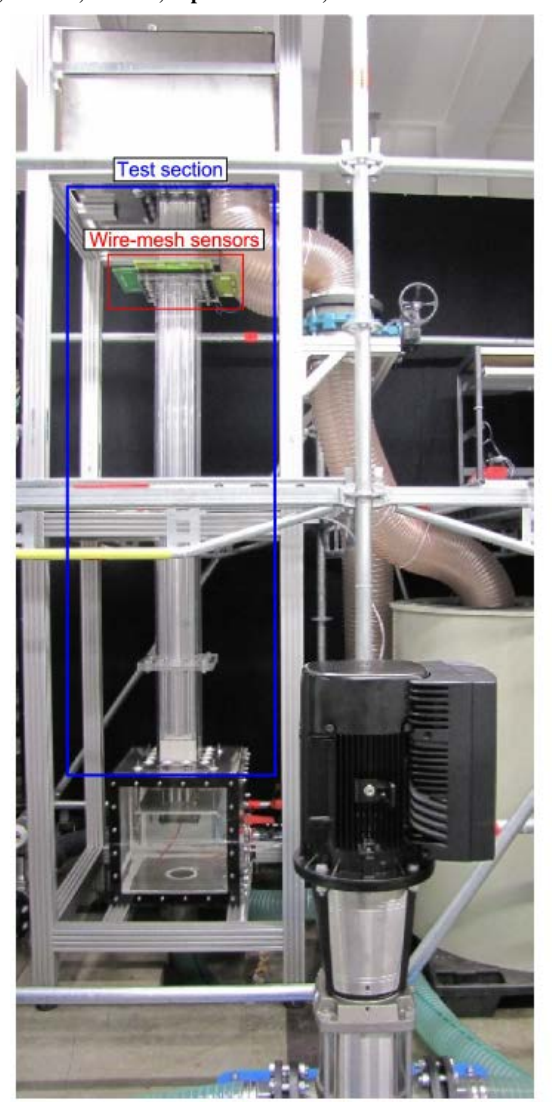
The test facility shown in Figure 4 was built at the Paul Scherrer Institute [27]. It is called SUBFLOW (= sub-channel flow). The core is a test section representing a matrix of 4 x 4 sub-channels in a square lattice of fuel rods. The dimensions were scaled up by a factor of 1:2.6 compared to typical PWR bundles (EPR). The test section is supplied by water at room temperature. For two-phase tests, air can be injected at the bottom. Capillaries mounted at different heights on the central rod simulator serve as injection nozzles for a salt tracer. The injection is carried out in an isokinetic way in order not to disturb the main flow by the momentum of the injected tracer solution.

2.2 Wire-mesh sensor for an application in the bundle model

As shown in Figure 5, it is possible to accommodate a wire-mesh sensor in the flow path of a fuel element bundle model [27]. The technical challenge consisted in the fact that the electrode wires must penetrate the fuel rod simulators in order to stretch over the entire free flow cross-section (Figure 5, left side). The fuel rod models were cut at the place of the wire-mesh sensor. Special plugs were fixed on both external sides of the grid planes. Between the grid planes, PVC pads were placed to keep a controlled axial distance between the wires. These plugs reunite the truncated rod simulators. The distance between both electrode grids of the sensor was 2 mm. Each has a matrix size of 64 x 64 crossing points. The lateral resolution is 2.125 mm. A top view of the sensor, together with the fuel rod models is shown in Figure 5 on the right side. Taking into account the scale, this corresponds to a resolution of about 0.8 mm with regard to the original dimensions of the lattice. It allows for accommodating a measuring matrix of 16 x 16 in each sub-channel. Across the sub-channel gap, there are four measuring points available in the lateral direction.

As shown in Figure 5, two sensors are mounted in an axial distance of 15 mm above each other. This enables measurements of the velocity by cross-correlation and time-of-flight techniques. The latter can be applied to fluctuations of the conductivity in a single-phase flow to measure the liquid velocity profile [27], as well as to gas bubbles to obtain the gas phase velocity [28].

The 14th International Topical Meeting on Nuclear Reactor Thermalhydraulics, NURETH-14 Toronto, Ontario, Canada, September 25-30, 2011



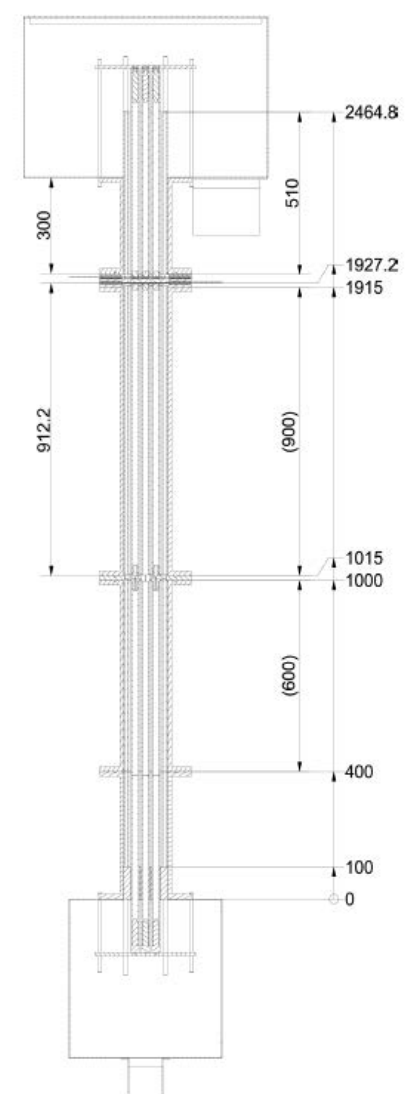


Figure 4 SUBLOW test facility at PSI representing a matrix of 4 x 4 sub-channels in a square fuel rod lattice typical for PWRs [27]

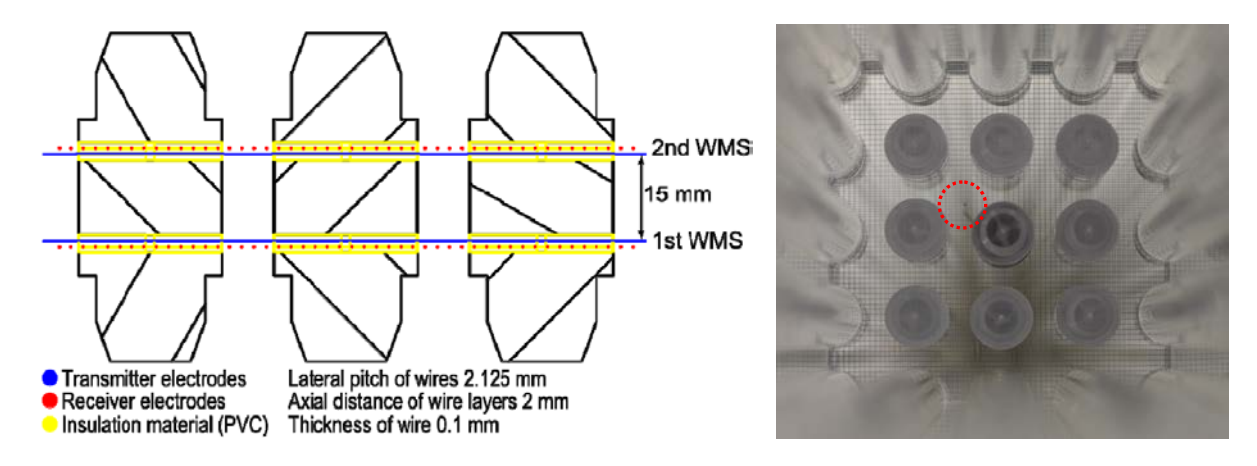


Figure 5 Construction of the pair of wire-mesh sensors applied to the rod bundle model [27] and top view of fuel rod simulators and one sensor (dashed red circle: injection capillary)

2.3 Results

Cross-mixing experiments were carried out by injecting water containing tracer salt into the center of one of the sub-channels. One of the capillaries for the injection is visible in the left upper sub-channel adjacent to the central rod in Figure 5 on the right side.

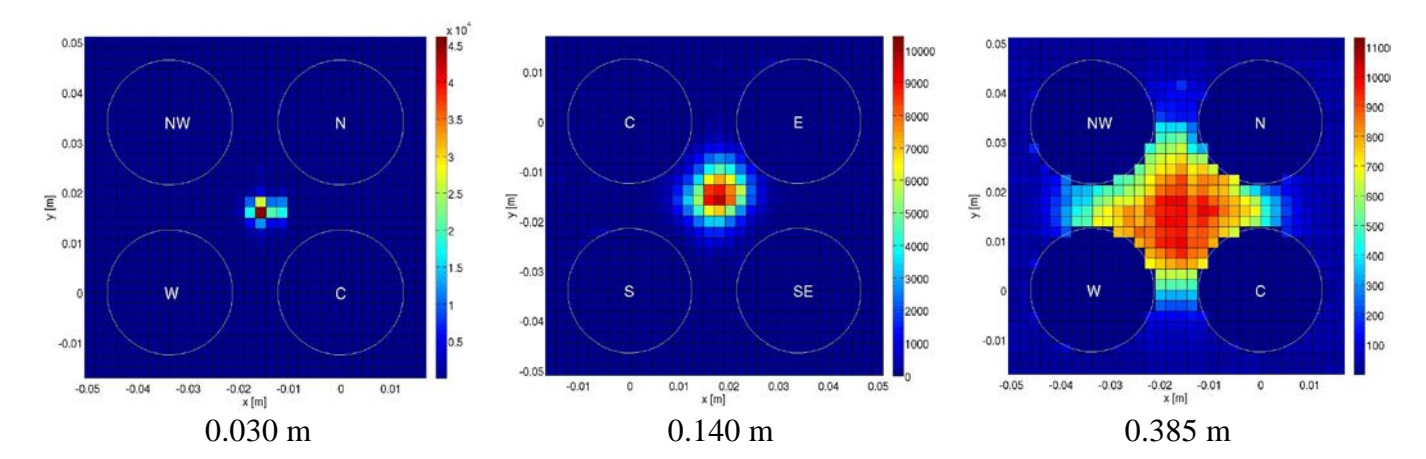


Figure 6 Time averaged distributions of the dimensionless tracer concentration (mixing scalar) at different distances downstream of the injection capillary at a liquid velocity of 1.2 m/s [27].

The tracer increases the conductivity, which is registered by the mesh sensor. In Figure 6, a time averaged distribution of the tracer concentration is displayed, measured at three different distances downstream of the injection. At a distance of 0.030 m, the tracer is still very much concentrated close to the location of the injection, whereas with growing distance the tracer cloud spreads out. At a distance of 0.385 m, a considerable part of the perturbation has already reached the neighboring subchannels. This lateral transport of the tracer is caused by turbulent dispersion. The experimental tracer profile for a larger distance (1.295 m), as well as the evaluation of concentration fluctuations, are discussed in the following section, where it is compared to the results of LES modeling.

2.4 LES modeling of turbulent cross-mixing in a single phase flow

For the unsteady solution of the Navier-Stokes equation by means of DNS and LES, the in-house code PSI-BOIL (Parallel SImulator of BOILing Phenomena) was developed [29]. It is designed to solve three-dimensional, single- and multiphase flow problems using the finite volume method. Fundamental modeling of non-adiabatic two-phase flows is the original purpose of PSI-BOIL. In this section, it is reported about the application of the LES solver to the single-phase cross-mixing case.

PSI-BOIL solves the Navier-Stokes equations with a staggered velocity discretization on a regular Cartesian grid, which makes the program very fast running compared to other CFD codes that are designed for unstructured grids, because a large number of arithmetical operations needed for the coordinate transformations can be saved. Furthermore, Cartesian grids allow very efficient parallelization. PSI-BOIL is written in C++ and uses Message Passing Interface (MPI) for parallel computations.

These advantages imply the use of immersed boundary techniques to reflect boundaries of the flow domains which do not coincide with the mesh lines of the Cartesian Grid. Simple porous body approaches, which rely on porosity factors defined for those cells that are cut by the flow boundary, are

not second order accurate, which is unacceptable from the point of view of best practice guidelines for CFD modeling. PSI-BOIL is therefore equipped with second order boundary conditions for the correct reflection of cut cells. The Navier-Stokes equation is solved on a staggered grid.

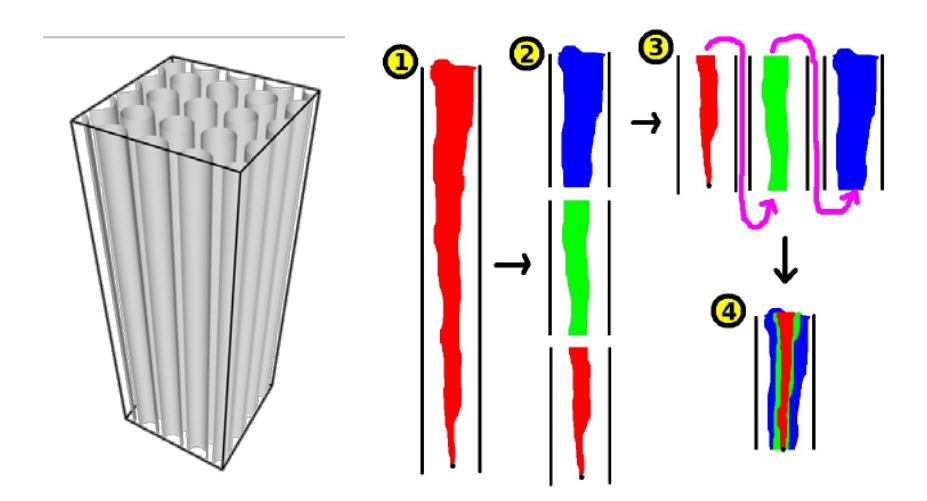


Figure 7 Fuel rod bundle of SUBFLOW represented by an unstructured grid with immersed boundary conditions (left), technique to solve the evolution of a neutral transport scalar exposed multiple times to a periodical transient velocity field calculated in this domain (right) [30]

The code was validated by calculating the tracer distribution in the SUBFLOW experiments [30]. The complex geometry of the fuel rod bundle was reflected in a rectangular Cartesian grid using the mentioned immersed boundary technique. The grid with the rods representing solid structures with noslip boundary conditions on their surface is shown in Figure 7 on the left side. The Navier-Stokes LES solver was coupled with a transport equation for the tracer. In order to keep computational costs as low as possible, the flow field was solved only in a small axial segment of the bundle model using periodic boundary conditions at the axial faces. In order to give the tracer distribution the freedom to evolve over a length corresponding to the height of the SUBFLOW bundle, the flow field was coupled with a set of multiple transport equations exposed to identical unsteady flow fields, but allowing for individual mixing processes. The concentration at the upper end of the domain found as a solution of the first transport equation was given as inlet boundary condition to the second one, and so on (Figure 7, right side).

The calculation was run with a time step of 0.1 ms. The results were accepted as converged after 120'000 time steps, i.e. after 12 s of process time. For the comparison with the experiment, the concentration field was averaged over another 35'000 time steps. Both, data from experiment and LES calculation have a sufficiently high time resolution to complement the time averaged concentration profiles with distributions of the RMS of the tracer concentration, which makes the validation of the model more sensitive. In Figure 8, both average concentration profiles and RMS distributions are compared for a quite well evolved mixing state at a distance of 1.295 m downstream of the injection nozzle.

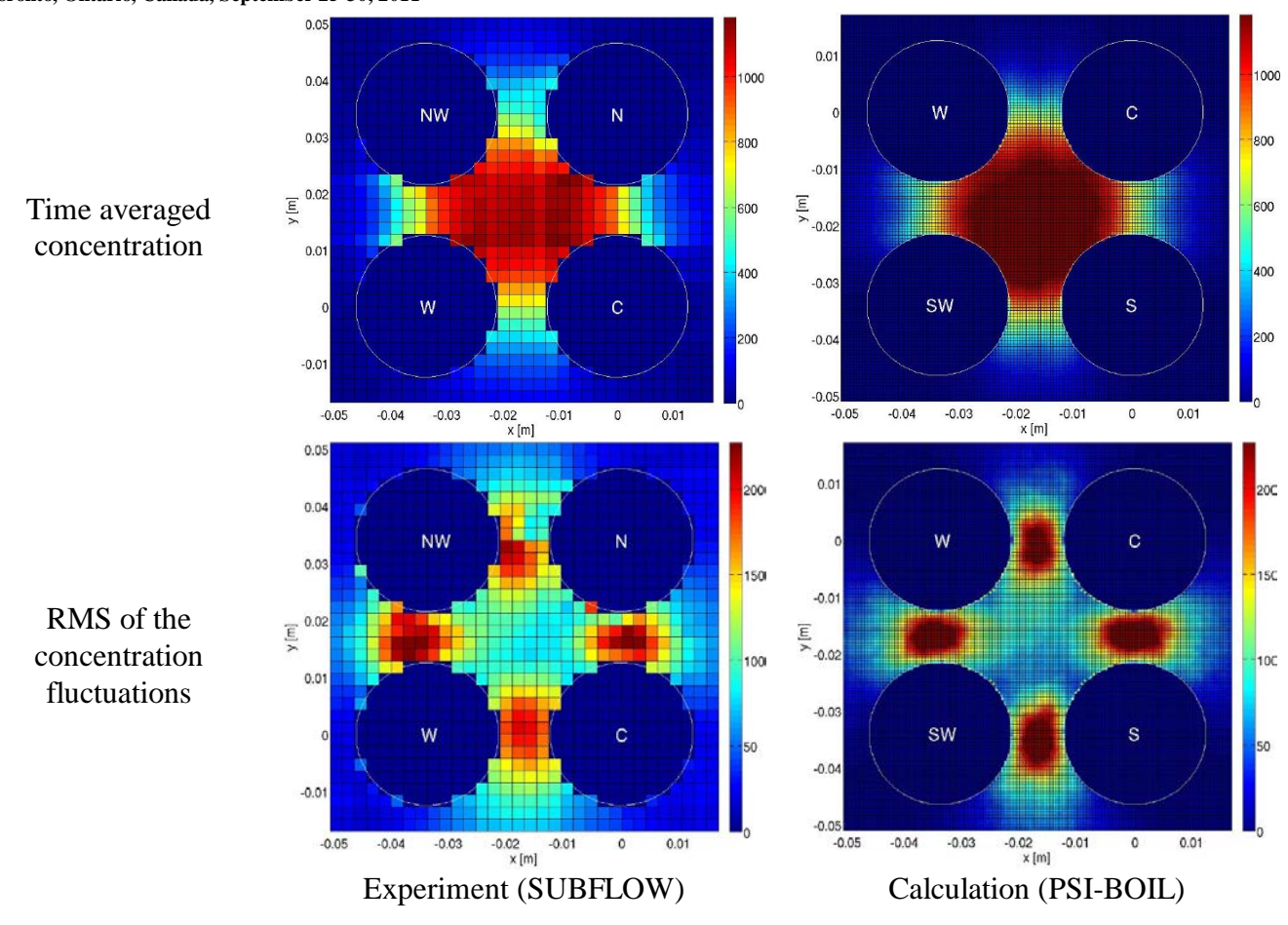


Figure 8 1.295 m downstream of the injection capillary at a liquid velocity of 1.2 m/s

A part of the tracer has already been transferred to the neighboring sub-channels, which is well reproduced by the calculation. A very good agreement has also been found for the amplitude of the concentration fluctuations, which displays a maximum in the sub-channel gaps, i.e. in the narrow place between neighboring sub-channels. This has been found to be typical of a progressed state of the cross-exchange. At lower distances from the injection, the RMS has a maximum in the center of the affected sub-channel, later this maximum declines and the maximum moves to the sub-channel gaps. The RMS indicates the intensity of the mixing process, which moves from the center of the sub-channel towards the sub-channel gaps. More results are found in [27] and [30].

3. Bubbly flow in fuel rod bundles

3.1 Experiments

The same wire-mesh sensor can of course be used for two-phase flow experiments [28]. For this purpose, air was injected into the lower part of the bundle. The air injection was performed by a set of small tubes, one in each sub-channel. In this way, we wanted to achieve a uniform gas distribution. A snapshot of the instantaneous gas fraction distribution showing several bubbles in the bundle is given in Figure 9, left side.

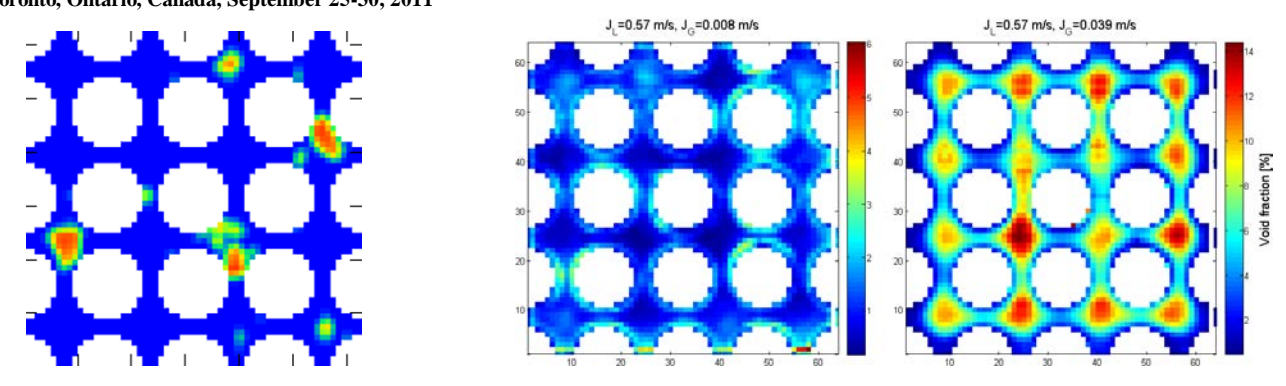


Figure 9 Snapshot of an instantaneous gas fraction distribution obtained by the wire-mesh sensor in the 4 x 4 bundle (left, blue – regions of high conductivity = water, red – low conductivity = air) and deduced time averaged void fraction distributions [28]

Two-dimensional void fraction distributions can be obtained by averaging over the time series of instantaneous gas fraction readings at each individual crossing point of two wires (Figure 9, right side). The boundary conditions for the results shown there differ in terms of the injected gas flow rate, while the liquid flow was kept constant. At the lower gas flow rate, pronounced wall peaks, i.e. an accumulation of the gaseous phase close to the surface of the fuel rod models is observed. This is due to the lift force, which in the liquid velocity gradient close to the wall pushes bubbles towards lower velocities, forming in this way the void maximum close to the surface where the non-slip boundary condition holds. The situation changes, when the air flow is increased. Now, the generated bubbles are bigger and the lift force changes sign. This effect was first observed and quantified for individual bubbles by Tomiyama [31] and later confirmed for a poly-disperse bubbly flow in a large vertical pipe [5]. The experiments presented here demonstrate that the phenomenon exists also under the conditions of a more complex geometry.

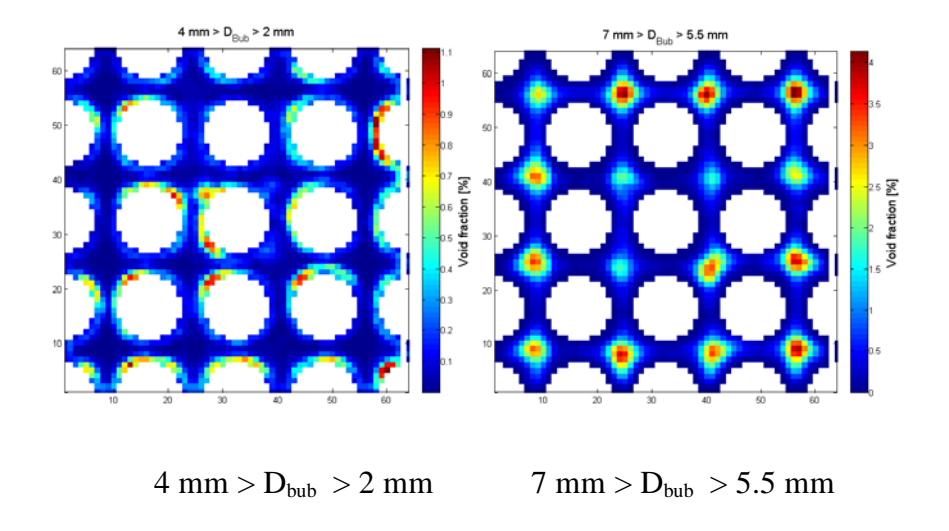


Figure 10 Average void fraction distributions decomposed according to bubble size ranges ($J_L=1.52$ m/s, $J_G=0.020$ m/s) [28]

There are numerous ways to process the wire-mesh data and extract secondary measuring information like bubble size distributions [32] or time averaged gas faction distributions decomposed into bubble size classes [33]. A corresponding result is presented in Figure 10. The first step is an identification of

bubbles as interconnected regions in the signal where the gaseous phase is present. By an integration of the volume of these regions, the equivalent bubble diameter is found. After this, an averaging is performed, which takes into account only portions of the instantaneous gas fractions that belong to bubbles of the chosen size. The result (Figure 10) shows that small bubbles are found close to the fuel rod surface and large ones in the center of the sub-channels in in multi-disperse flow containing bubbles both larger and smaller than the critical diameter for the lift force reversal.

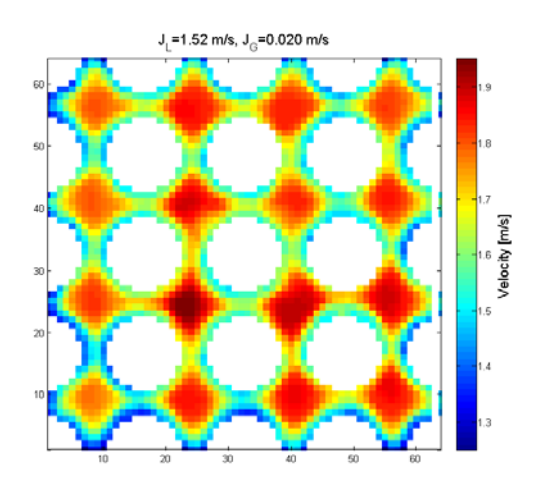


Figure 11 Bubble velocity profile obtained by a time-of-flight measurement with subsequent averaging over a large ensemble of bubbles [28]

As explained earlier, the bundle model is equipped with a pair of wire-mesh sensors, placed at a distance of 15 mm behind each other. This allows for a measurement of velocities, both for single and two-phase experiments. Bubble velocities can be measured either by a cross-correlation of the signals of both sensors at the identical location within the sensor matrix or by a time-of-flight detection carried out for individual bubbles after their identification. A typical result of the second approach is shown in Figure 11, where individual velocity readings are averaged over a large measuring period. The profile of the gas phase velocity in the sub-channel is clearly visible.

3.2 Modeling of bubbly flows

For two-phase simulations, PSI-BOIL, which was introduced as a LES/DNS solver in section 2.4, is equipped with a surface tracking algorithm for the gas-liquid interface. It is based on a transport equation for the color function defining the position of the interface in space and time. Second order numerical methods (CIP-CSL2 =Constrained Interpolated Profile method: Conservative Semi-Lagrangian 2nd order scheme, [29]) suppress unphysical deteriorations of the shape of the gas-liquid interface due to grid effects, numerical diffusion and parasitic currents. With PSI-BOIL it is possible to reproduce the adiabatic experiments. The code has already demonstrated the capability of simulating a transient flow of multi-disperse deforming bubbles that can coalesce when colliding (Figure 12). The use of a transport equation for a color function has the advantage that the numerical efforts do not grow with increasing number of bubbles present in the modeling domain. Next step will be the comparison with the experimental results from the SUBLOW bundle. This work benefits from the implementation of immersed boundary conditions discussed in section 2.4, since this is necessary to reflect the fuel rod bundle geometry also in the two-phase calculations.

The 14th International Topical Meeting on Nuclear Reactor Thermalhydraulics, NURETH-14 Toronto, Ontario, Canada, September 25-30, 2011

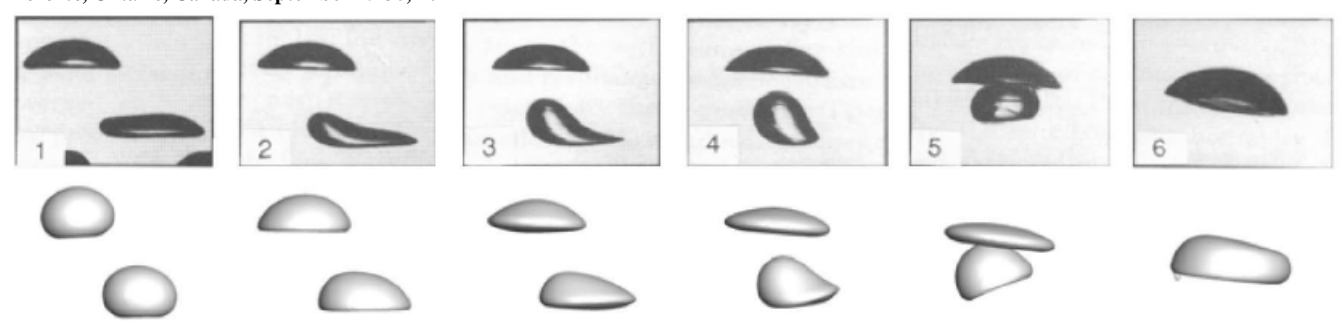


Figure 12 Sequential snapshot of oblique coalescence of experimental data (top) and computed results (bottom). Time difference between the frames is 0.03 (s). Eo=16, Mo=0.0002 [29], experimental data:

Brereton [34]

Recently, the code was equipped with an algebraic model of the bubble contact line, which takes into account the adsorption layer of water underneath the bubble and the high-curvature region of the transition from the adsorption layer to the free surface, where most of the heat transfer happens. With this model, it was possible to calculate the growth, departure and terminal rise of a vapor bubble under pool boiling conditions (Figure 13). This is the first step towards a flow boiling modeling, which, in the long term, is intended to shed light on the phenomenon of departure from nucleate boiling.

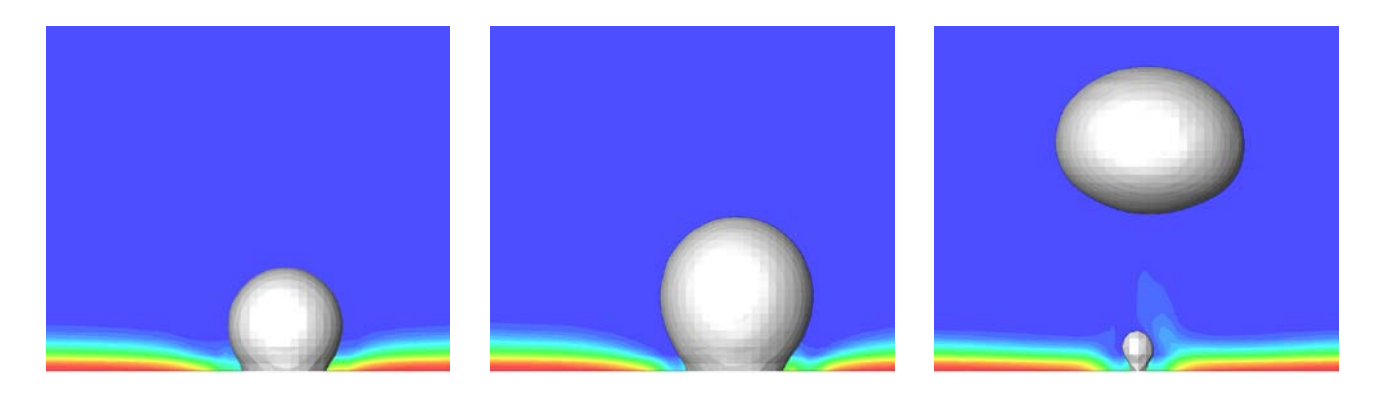


Figure 13 Pool boiling simulation performed with PSI-BOIL (preliminary results by Sato and Niceno, grey – gas-liquid interface, color code: temperature in the liquid phase)

The long-term goal of the theoretical work is a multi-scale approach integrating molecular phenomena at the interface where phase transition takes place. A promising approach consists in the application of a phase field function [29].

4. Annular flow in fuel rod bundles of boiling water reactors

4.1 Cold Adiabatic double sub-channel model

For studying the annular flow in fuel elements of boiling water reactors, the test loop shown in Figure 13 was built [35]. The loop operates close to ambient pressure and temperature. It is closed for both liquid and gaseous phases. The gas is circulated by means of a compressor. The latter has the

advantage that different gases can be applied without the need to release them to the atmosphere. Experiments were performed with helium, air and octafluorocyclobutane (C_4F_8).

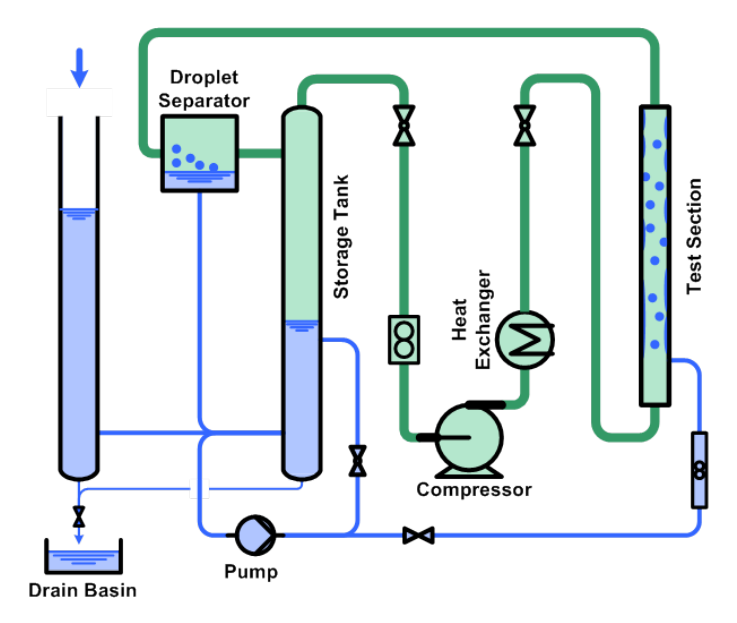


Figure 13 Test loop CALVIN for annular flow studies in fuel elements of boiling water reactors [35]

The test section consists of a vertical channel made from two half-shells of acrylic glass. The flow channel itself has the shape of two neighboring sub-channels (Figure 14). This is the minimum configuration which is needed to study the flow in a sub-channel together with the exchange via the sub-channel gap.

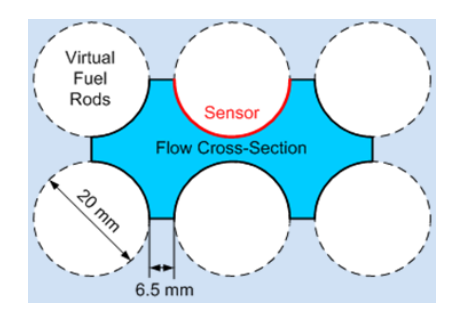


Figure 14 Geometry of the double sub-channel model of a BWR fuel rod bundle

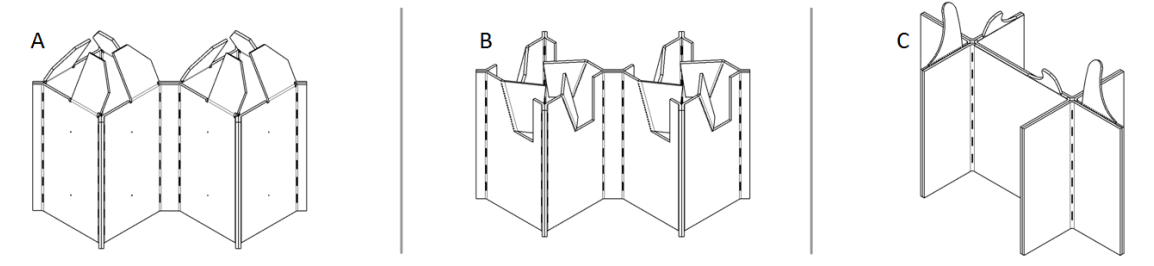
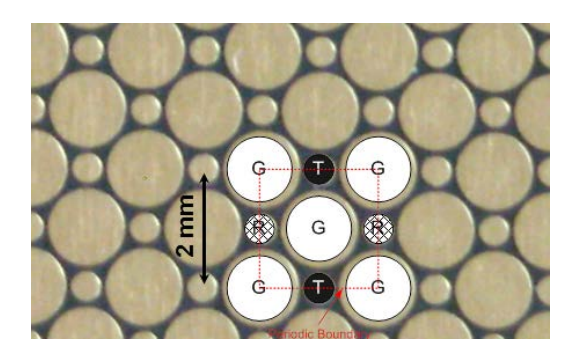


Figure 15 Three different generic models of functional spacer grids

The construction allows to place models of spacer grids into the flow channel. Three different generic spacer geometries were tested (Figure 15), which are equipped with flow controlling vanes.

4.2 Electrical liquid film sensors

The electrical film sensor used in the annular flow experiments consists in a matrix of the size 16 x 64, which is sampled with a frequency of 10 kHz. The electrode arrangement is shown in Figure 16 on the left side.



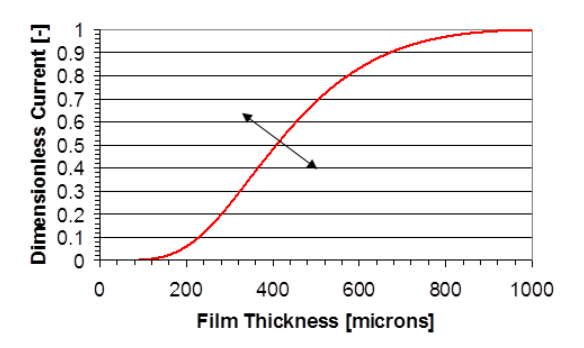


Figure 16 Electrode islands of the liquid film sensor (left, G – ground electrode, T – transmitter, R – receiver) and characteristics of the sensor (right)

The current is depending on the thickness of an electrically conducting liquid film covering the surface of the sensor at the position of both electrodes. Potential field calculations have shown that the current reaches saturation at a certain liquid film thickness. This has been confirmed by calibration measurements. The characteristic of the sensor is shown in Figure 16 on the right side. The saturation at about 800 μ m is clearly visible. The shape of the characteristics can be modified in the direction of the black arrows by changing the diameter of the grounded pads. In general, grounded areas between transmitter and receiver islands push the potential lines away from the sensor surface. The size of the grounded islands applied in case of the sensor on Figure 16 causes the small sensibility in the region of film thicknesses below 200 μ m, but allow stretching the upper limit to a higher film thickness. A decrease the size of the ground pads results in a shift of the characteristic to the left, while increasing them shifts the curve to the right.

The sensor can be manufactured as a flat plate, but also on a bended surface, when a flexible printed circuit board technology is used for its manufacturing [35]. For experiments in a flow channel representing a pair of neighboring sub-channels of a BWR fuel rod bundle, a bended sensor was mounted on the semi-cylindrical surface of a fuel rod model, as shown in the drawing of the cross-section of the double sub-channel model in Figure 14. A photo of the sensor itself is presented in Figure 17.



Figure 17 Bended film sensor on top of a semi-cylindrical fuel rod model

The diameter of the fuel rod model is 20 mm, which is about twice the diameter of a real BWR fuel rod. It was decided to upscale the sub-channel, because it is easier to achieve high Reynolds numbers at

cold laboratory conditions, where the liquid viscosity is much higher than in the real reactor. The arrangement of the sensor in the double sub-channel, which consists of two half-shells, is shown in Figure 18 on the right side.

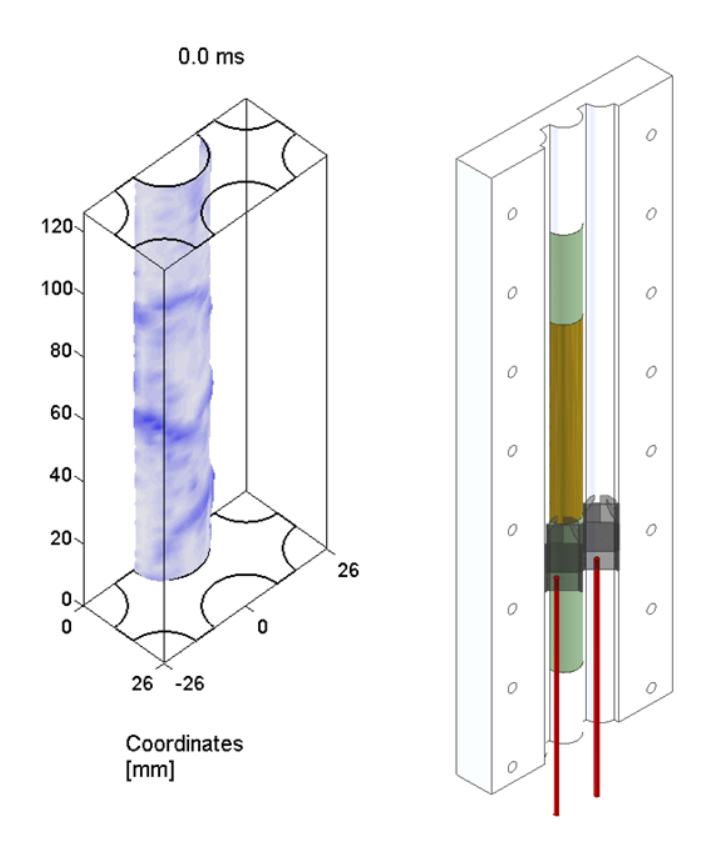


Figure 18 Film sensor and spacer model in the half-shell of the double sub-channel model (right) and snapshot of the instantaneous liquid film thickness in a test without spacer (left), air velocity: 40 m/s, volumetric flow ratio of water: 2 %

4.3 Dynamic liquid films

On the left side of Figure 18, a snapshot of the film thickness distribution is shown for a case without spacer grid. Thanks to the high time resolution combined with the two-dimensional measuring matrix, the dynamic behavior of the liquid film is accessible. A number of different digital processing methods was proposed, applied to the signals of the sensor and reported in [36]. Besides a statistical evaluation revealing the average film thickness and the liquid holdup profile in the film, which allows for distinguishing between base film and wave region, advanced algorithms for a decomposition of the wave signal in time and spatial domain is proposed. The result consists in an identification of shape parameters and a propagation velocity value for each wave individually. By a statistical correlation of this data the dependency of the wave velocity from wave height was characterized. By tracking the waves on the two-dimensional domain of the sensor surface, wave trajectories were found. These trajectories are straight for the case without a spacer grid, but deform and bend due to the effect of the spacers, in particular the vanes, on the gas flow field driving the liquid film.

A large series of experiments on the effect of the different generic functional spacers shown in Figure 15 was conducted. The most important result consists in a complete mapping of time-averaged film thickness distributions along the surface of the fuel rod for all spacer grid versions and three different gas densities. As an example, the influence of spacer B is shown in Figure 19.

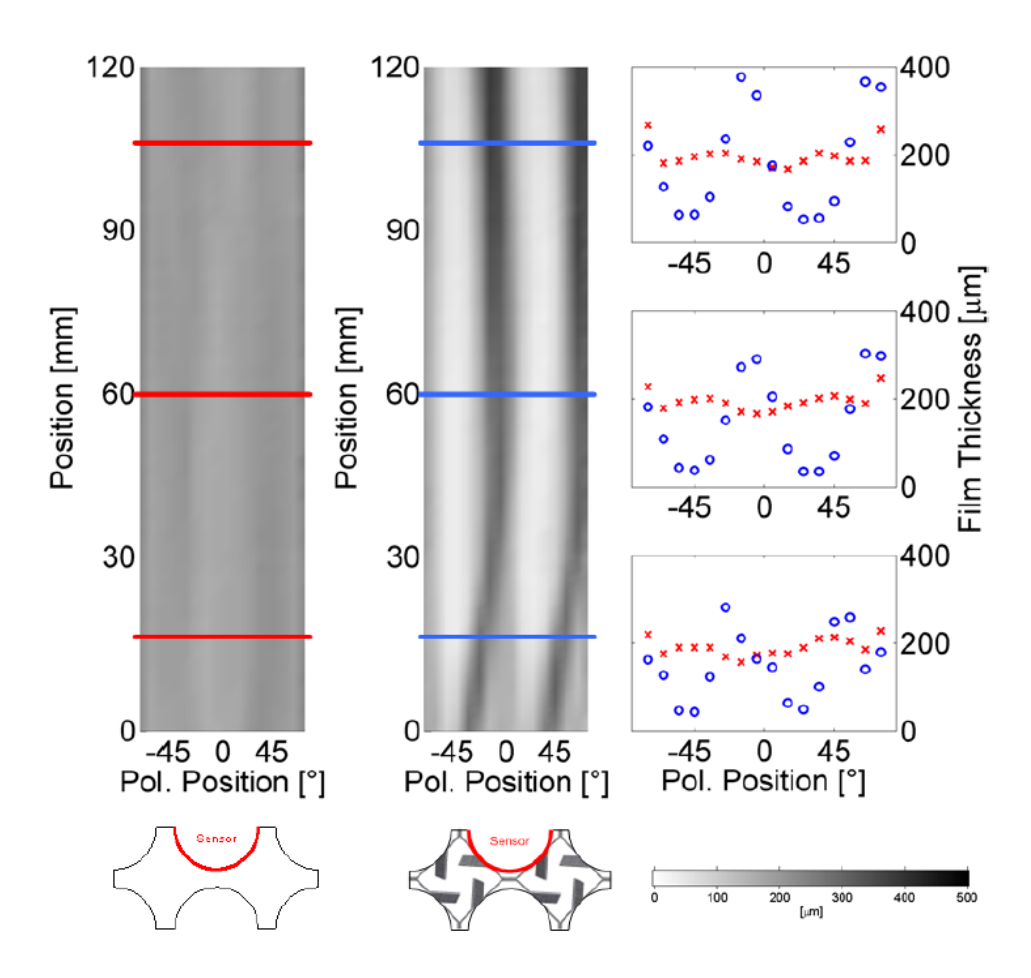


Figure 19 Visualization of time averaged film thickness: distribution without spacer (left) and spacer B (center), profiles at various axial positions (right), flow parameters: J=50 m/s, $1-\beta=0.004$, air-water

In the experiments conducted at the CALVIN facility, it turned out that droplet impacts on the liquid film generate a characteristic signature in the time-resolved sensor signal. The residuum of an autoregressive model has shown to be a sensible indicator for a droplet impact. The model trained to the unperturbed wavy structure of the film produces a strong increase of the residuum, when a droplet impact disturbs these structures. This effect can be amplified by adding salt tracer to artificially injected droplets. Furthermore, the intensity of the continuous increase of the conductivity in the liquid film, related to the conductivity of the film without tracer addition to the droplets, can be used to quantify the total amount of deposited liquid. Both methods were used by Damsohn [35, 36] to characterize the enhancement of droplet deposition by functional spacers.

4.4 Tomographic imaging of the double sub-channel with cold neutrons

The first intension to perform neutron tomography of the annular flow in the geometry of the pair of sub-channels used in the CALVIN loop concerned an independent validation of the film thickness

measurements by the electrical sensor. Since small quantities of water have to be detected, the stronger attenuation of cold neutrons compared to thermal neutrons was seen as an advantage to achieve a good contrast. A test channel with the same flow cross-section as it was used in the previous sections (Figure 14) was manufactured from aluminum, which is a material with one of the lowest total cross-sections with cold neutrons [37]. The test channel was accommodated in the hut of the ICON beam-line at the spallation neutron source SINQ of PSI, as shown in Figure 20.

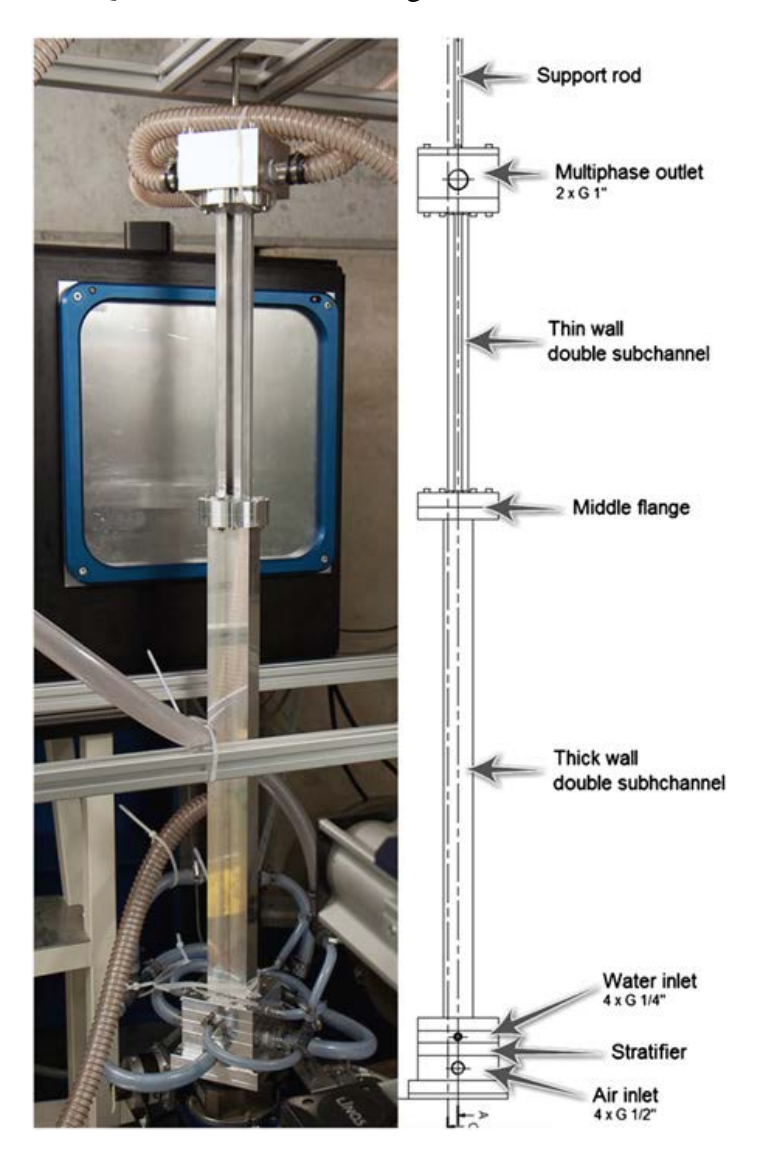


Figure 20 Test channel consisting of a pair of neighboring sub-channels arranges in front of the twodimensional neutron camera in the shielding hut of the ICON beam-line at PSI [37]

In the upper part, where the transmission of the neutron beam is recorded, the wall thickness was reduced to 3 mm to avoid unnecessary attenuation in the aluminum. The entire test channel was mounted on a rotating table, because tomography requires an acquisition of radiograms from a large set of different directions. The air and water supply was arranged through flexible tubes.

The cross-section of channel, together with one of the tested spacer models, is shown in Figure 21. The 3 mm thick aluminum walls are painted grey. Experiments were carried out with and without functional spacers. The neutron flux was 3.10^6 1/(cm²s). A field of view of 65x65 mm² was covered by

a 1024x1024 pixel ANDOR CCD camera. The neutrons were converted by a 100 μm thick ZnS(Ag)+6LiF scintillator screen based on an (n,α) reaction. For each tomogram, a set of 375 projections was recorded. For this purpose, the test section was rotated in steps of 360/375 deg. The integration time was 30 s per projection, which means that a full tomogram was available after a measuring time of about 3 hours.

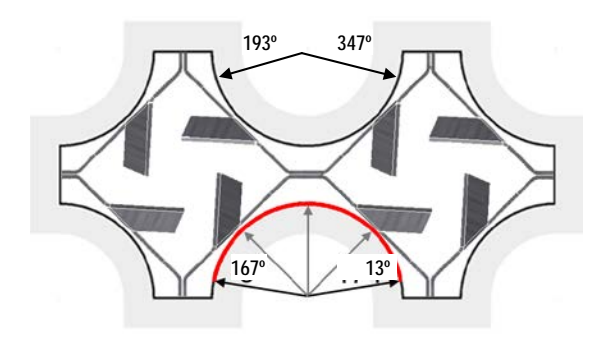


Figure 21 Cross-section of the double sub-channel model used for cold neutron tomography with functional fuel rod spacer

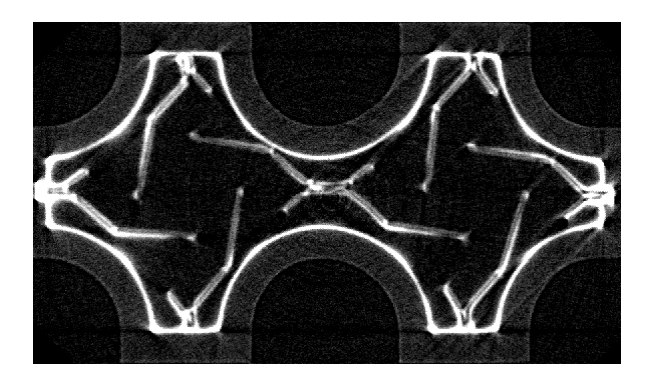


Figure 22 Typical tomogram of the neutron attenuation in the double sub-channel geometry [37]

A typical result is shown in Figure 22. The highest contrast is produced by the water film, both on the channel walls and the spacer structures. The aluminum is seen as a very weak grey area. The resolution is surprisingly good; the spacer elements display a characteristic sandwich structure water-aluminum-water with a dark stripe in the center. The changing film thickness along the circumference of the fuel rod models is clearly visible.

Despite of the fact that the blurring of the whole imaging system is about 385 μ m at a pixel resolution of 64.2 μ m, it is possible to evaluate a liquid film thickness with a much higher resolution. This is done by calibrating the grey values to the attenuation of plain liquid, and integrating the local water holdup and interpreting it as a quantity of liquid wetting the wall. This was applied to study the influence of the spacer vanes to the liquid film thickness distribution downstream of the spacer. A result for the spacer geometry shown in Figure 21 is presented in Figure 23.

In case of ICON, the images are two-dimensional radiograms. The tomographic reconstruction is therefore delivering a three-dimensional attenuation distribution inside the object. The distribution of the liquid film shown on the left side of Figure 23 is therefore the result of a full measuring run. The

comparison with time averaged liquid film thickness data obtained by the electrical sensor introduced earlier is very good. The advantage of the neutron tomography consists in a higher spatial resolution and in the fact that liquid can be detected not only on the surface of a sensor, but everywhere in the channel, including the complicated spacer structures and the bulk flow [38]. The advantage of the electrical film sensor, on the other hand, consists in its very high time resolution of 10 kHz, which provides access to transient structures like waves and droplet impacts.

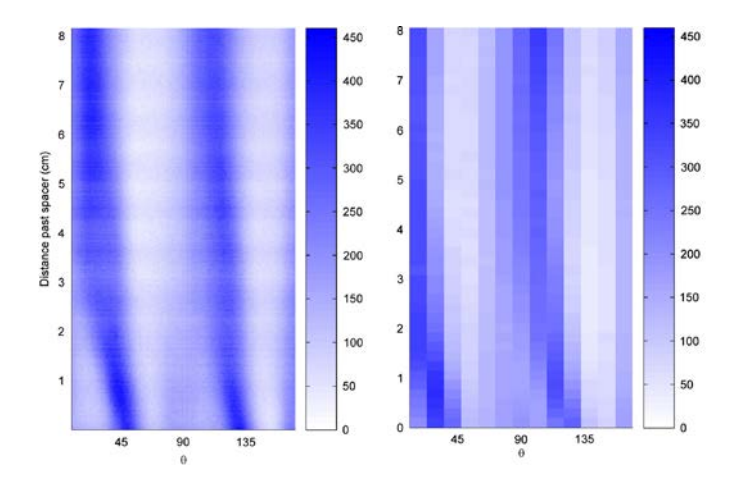


Figure 23 Comparison of time averaged film thickness on the semi-spherical fuel rod model in the double sub-channel of Figure 21, left: neutron tomography, right: conductance film thickness sensor

A particular result demonstrating the advantage of the given neutron tomography is shown in Figure 24. By a differential tomography, where first an image of the dry aluminum structures was taken, which was later on subtracted from the image obtained during the experiment with air and water injection, it was possible to quantify the thickness of the water layer on top of a spacer vane. Water is found mainly on the back sides of the vanes (left image) where the shear stress is low, and in the wake above the rear edge of the vanes [38]. The white contour shows the edge of the vane.

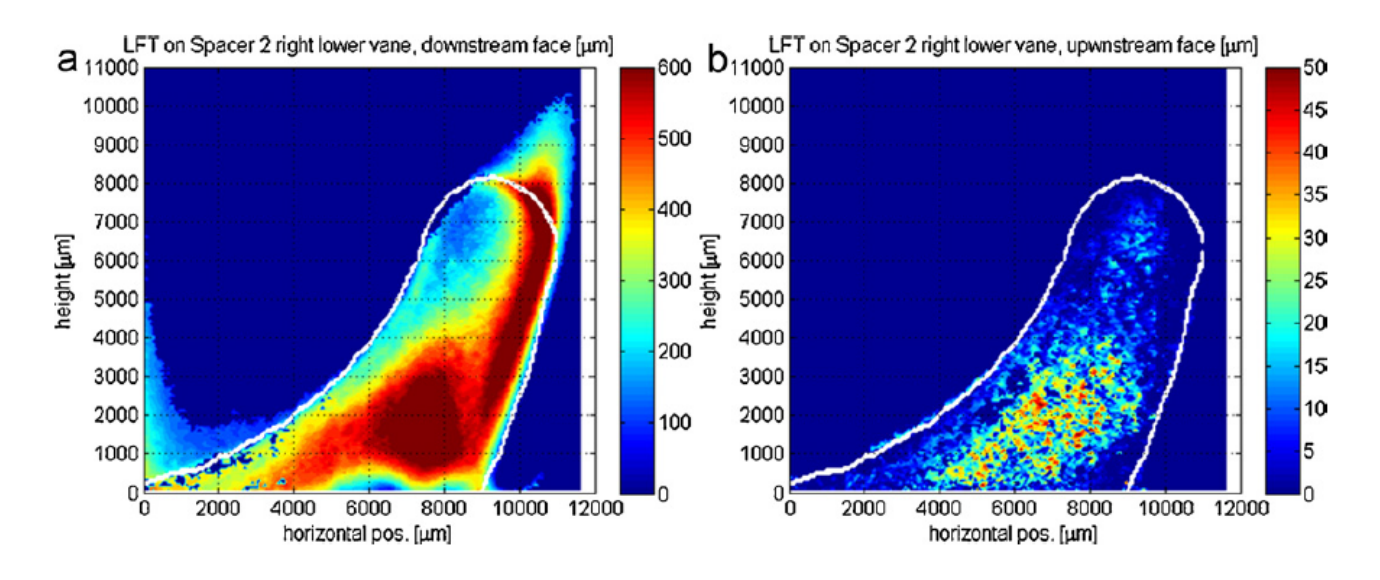


Figure 24 Liquid film thickness distribution on the downstream surface (a) and on the upstream surface (b) of the lower-right vane of Spacer C (see Figure 15), [38]

4.5 Outlook: Feasibility study on tomography with fast neutrons

In the future, the application of a pulsed plasma fusion source for imaging with fast neutrons is planned. The source is based on a D-D reaction and can produce about 10^8 1/s neutrons.

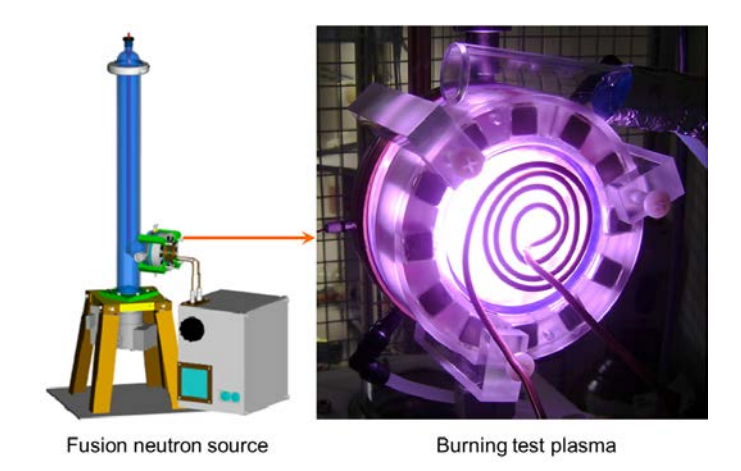


Figure 25 Plasma fusion neutron source (left) and photo of the burning test plasma (hydrogen)

Deuterium ions are extracted from a burning deuterium plasma and accelerated with 150 kV towards the titanium target, where the fusion reaction takes place with already deposited deuterium atoms. Since pulses can be generated by an electrical control of the extraction, short exposure times can be reached. Since the flux of neutrons is too small to obtain a good imaging quality with during a single exposure, a phase-lock technique is envisaged to visualize periodic processes. The project is in the state of a feasibility study. One of the main concerns is the efficiency of detectors for fast neutrons. A view of the source and the burning test plasma (hydrogen) is shown in Figure 25. A special feature is a neutron emitting spot of only 2 mm diameter, which is small compared to D-D and D-T neutron generators that are commercially available.

4.6 Modeling of the time-averaged film thickness distribution

Since the time-averaged liquid film thickness distribution is strongly influenced by the spacer geometry, a theoretical prediction of the spacer effect is very interesting for scoping studies. Spacer geometries can be preselected from the point of view of creating favorable conditions for a reliable wetting of the fuel rod surface. Vane geometries that deteriorate the film thickness can be identified and discarded before experiments have to be performed.

It was decided to explore the possibilities to set up simplified models for the time averaged film thickness that are capable in reflecting the spacer effect with the lowest possible numerical effort. Such a model was found by Damsohn [39] by a calculation of the three-dimensional velocity field in the gas core of the annular flow and a coupling to a two-dimensional liquid film model via the shear stress distribution at the gas-liquid interface. The following simplifying assumptions were taken:

- The flow both of the liquid and the gaseous phases was assumed to be steady-state.
- The gas flow field was modeled by means of steady-state RANS, applying the k-ɛ turbulence model, whereas the presence of the liquid film was not taken into account, i.e. a no-slip

boundary condition was set to the gas flow that is identical to the solid wall of the flow channel given by the fuel rods and the spacer structures.

- The liquid film flow is assumed to be driven by the shear stress acting from the gas flow on the solid boundary.
- A fully established laminar viscous liquid flow resulting in a linear velocity profile within the film was assumed. Inertia of the liquid phase was neglected.

In reality the structure of the liquid film is rather far from being a laminar flow, since there is a base film that may be partially turbulent, overlaid by different kinds of waves. The viscosity needed in the film model is therefore different from the molecular viscosity. It is treated as a model parameter, which is fitted to obtain the measured time-averaged film thickness in the sub-channel without spacer from the shear stress calculated for the same case. It is assumed that the value found in this way can be accepted as a good approximate for the case of the flow structure generated by the presence of the spacer. Further model components are an empirical turbulent dispersion coefficient [39] and a virtual surface tension limiting the curvature of the film [36]. As shown in Figure 26, the most important element of the model is the two-dimensional transport equation of the liquid mass in the film, which is driven by the local shear stress at the interface. The turbulent dispersion and the curvature limitation (not shown in Figure 26) only gradually improve the agreement with the experiment.

Models connecting the film thickness with the shear stress at the gas-liquid interface are known e.g. from Kishore [40], who calculated the film thickness based on the assumption that the liquid mass flow in the film stays uniformly distributed. This leads to a strong underestimation of the influence of a non-uniform shear stress distribution, as shown in Figure 26 (one-dimensional model), too. In fact, in regions where the vector field of the shear stress on the interface has a positive divergence, it has to be expected that the liquid mass in the film follows this divergence and is pushed out of this region. The model of Damsohn (see also [36]) belongs to the class of models taking into account the mass redistribution in the film, like the ones of Tso & Sugawara [41] and Bai & Gosman [42], the latter being implemented in the commercial CFD code STAR-CD.

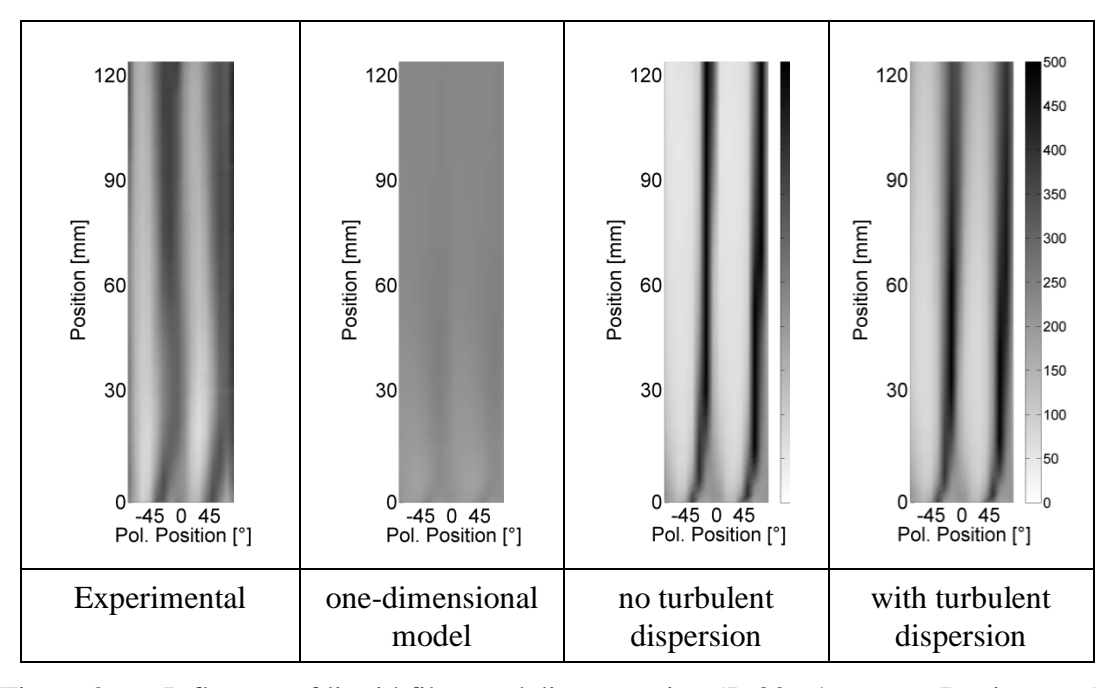


Figure 26 Influence of liquid film modeling equation (J=30m/s, spacer B, air-water)

The merits of the work of Damsohn [36] consist in a very comprehensive validation of the model and a detailed sensitivity study highlighting the relevance of the individual model components and simplifying assumptions. It was shown that one fixed set of model parameters can provide a satisfying agreement with the experiments over a large range of gas densities, flow rates and spacer geometries. This is illustrated in Figure 27, where both measured and calculated averaged film thickness profiles are presented for all three spacers and all three gases.

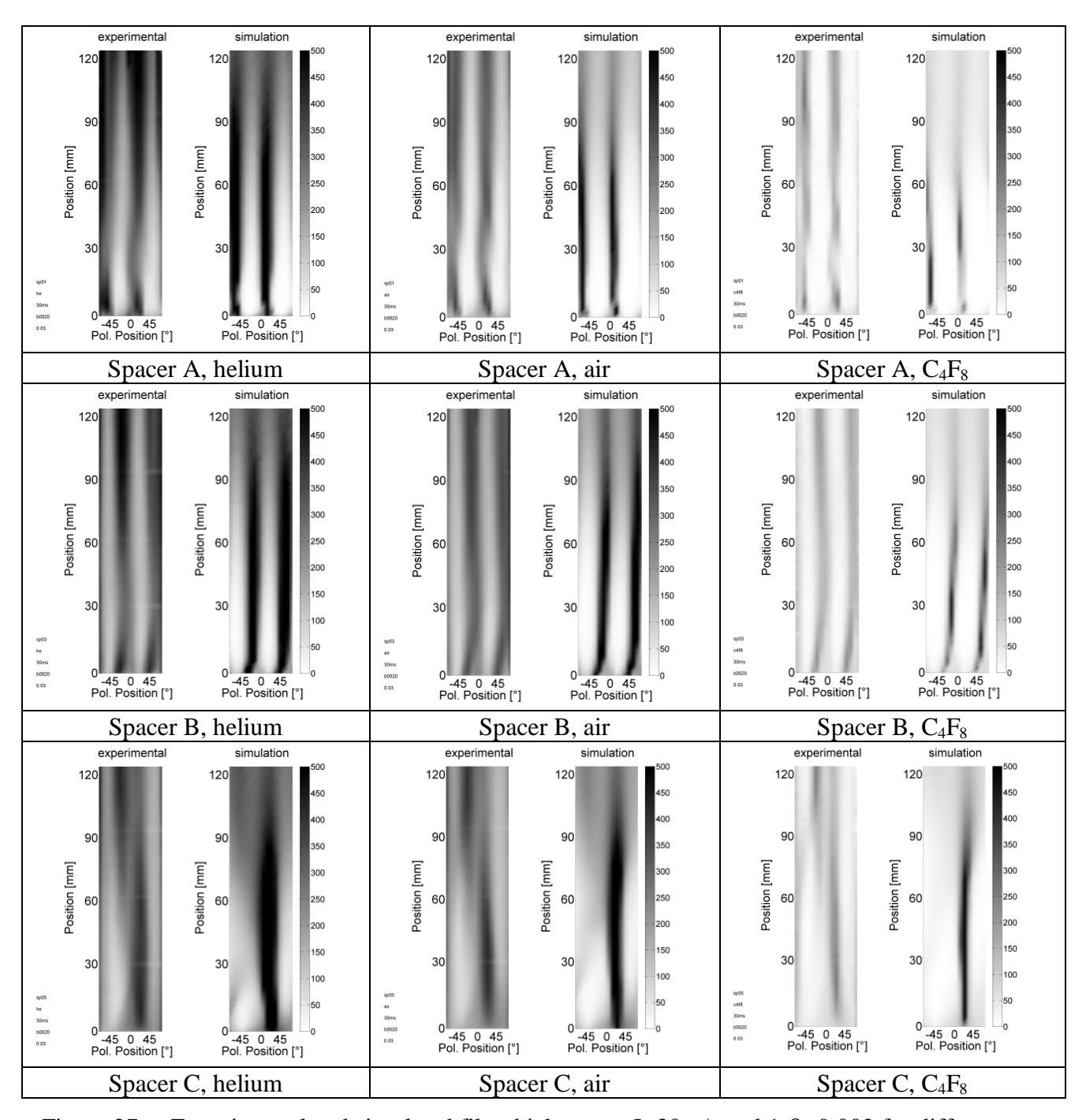


Figure 27 Experimental and simulated film thickness at J=30m/s and 1- β =0.002 for different spacer geometries and gases (model parameter: turbulent diffusion coefficient D = 3e5 m²/s)

Both pattern and quantitative values of the film thickness distributions are reproduced in a satisfying way, sufficient for using the theoretical method in scoping studies on the optimization of spacers. Bigger deviations are observed for spacer type C, where the transition of the streak of high film thickness from the right into the left sub-channel (the sub-channel gap is in the middle of the plots) around a distance of 60 - 90 mm from the spacer is not reproduced by the model, i.e. there is of course room for future improvements. The experiments have revealed a strong density effect, leading to a thinning of the film with growing gas density. The fact that this is well reproduced by the model is trivial, since link between film thickness and local shear stress from the RANS calculation is calibrated on the unperturbed film thickness in case of the absence of a spacer grid.

5. Two-phase flows and liquid films in narrow channels

In the course of the development of high-conversion light water reactors, the reduction of the moderator-to-fuel ratio (MFR) is crucial to reach a hard neutron spectrum in the reactor. This is done by reducing the distance between fuel rods and by introducing a triangular fuel rod lattice instead of the usual square lattice. The remaining gap for the coolant flow becomes quite narrow, i.e. the gap becomes commensurable with the bubble size. This challenges the two-phase models. The observation of bubbly flows in narrow gaps is therefore of considerable interest in order to validate the analysis tools.

To approach the problem, experiments in a flat narrow channel with liquid film sensors at the front and back walls were performed [44]. The use of two opposite sensors is a combination of both options of electrodes at the channel wall described before (Figure 28, left). Transmitter electrodes were provided with voltage pulses only on one side of the channel. The current received on the opposite side characterizes the conductance across the narrow gap. In this measuring information, shape and size of gas bubbles are reflected as regions of low conductance. The signal received on the same side where the transmitter is, can be used to characterize the covering of the surface with water. In this way, the liquid film thickness underneath gas bubbles in a narrow rectangular gap was measured for the first time. The channel is shown in Figure 28, right side.

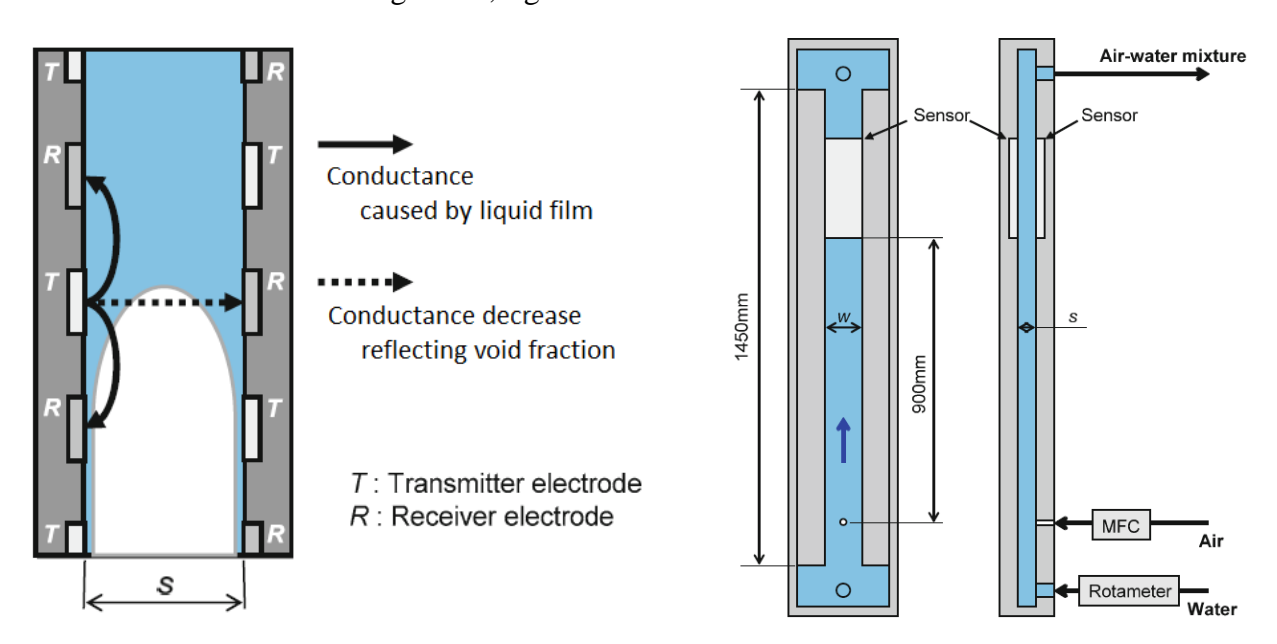


Figure 28 Principle of the use of two opposite film sensors (left) and front and side views of the narrow rectangular channel (right, w = 32 mm, s = 1.5 mm)

The capability to characterize the remaining liquid film during the passage of a gas bubble is illustrated for the case of a coalescence of a pair of cap bubbles in a slug flow (Figure 29). Before the coalescence, the water slug separating both bubbles moves fast in an upwards direction, because it is driven by the fast gas flow. When the coalescence happens, the water inventory of the slug is found in the liquid film. Subsequently, this additional portion of water is clearly seen to slowly draining downwards, while the upwards flow of the gas phase continues.

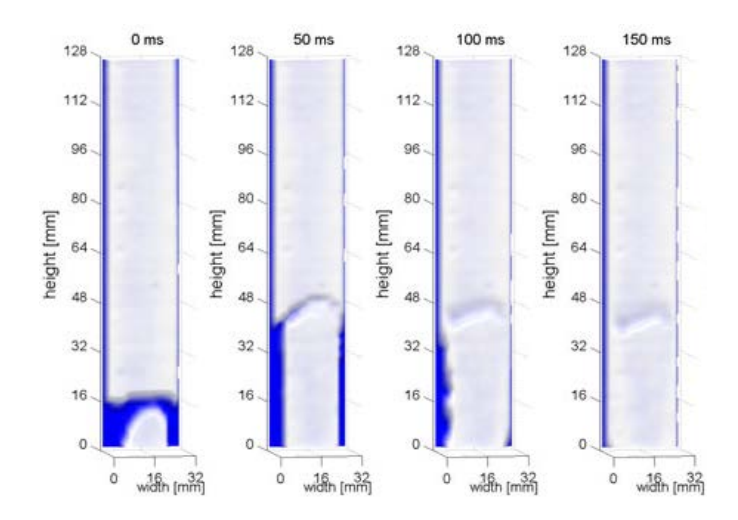


Figure 29 Coalescence of a pair of cap bubbles in the narrow gap with a subsequent drainage of the residual liquid from the collapsed water slug [44]

An interesting observation was made concerning the lateral film thickness profile underneath a bubble, as shown in Figure 30. The film thickness regularly showed minima at the left and right side of the bubble, while the thickness in the center is significantly higher. As it can be seen, this phenomenon of a dimpled film was only observed in the horizontal direction. Over the height, the film thickness distributions were found to be more or less uniform (Figure 31).

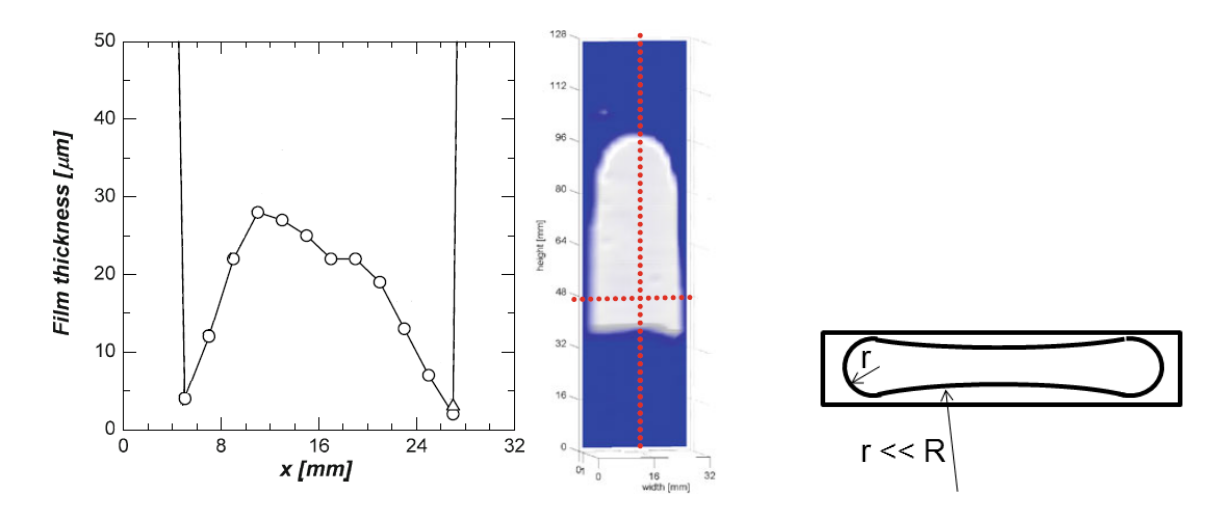


Figure 30 Cap bubble in the narrow gap (middle) and dimpled horizontal profile of the liquid film thickness between bubble and wall (left) [44], interpretation of measuring data (right)

The 14th International Topical Meeting on Nuclear Reactor Thermalhydraulics, NURETH-14 Toronto, Ontario, Canada, September 25-30, 2011

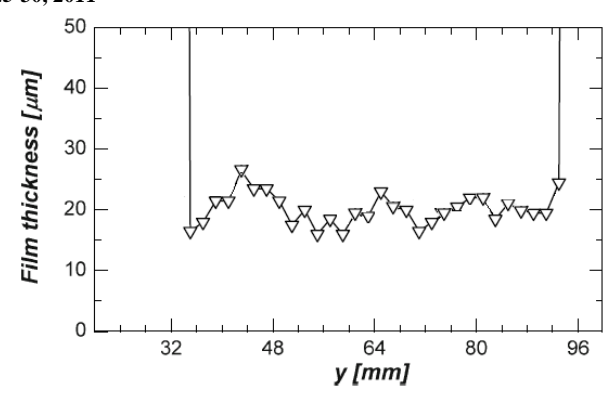


Figure 31 Liquid film thickness profile between the cap bubble and the channel wall along the vertical red dashed line in Figure 29 [44]

As a next step, the implementation of the technique into a sub-channel model of a narrow fuel rod bundle with a triangular lattice is planned (Figure 32).

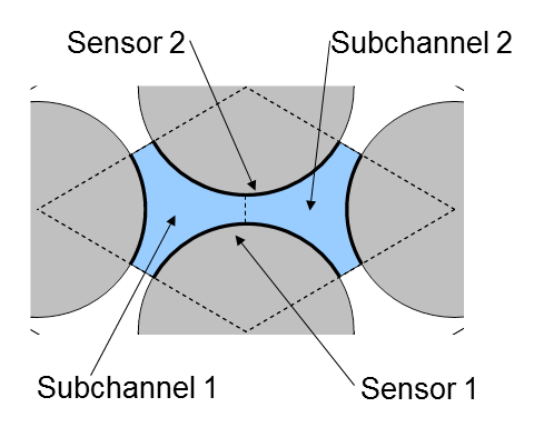


Figure 32 Cross-section of a pair of neighboring cooling sub-channels in a fuel rod bundle with a dense triangular lattice

6. Conclusion

Wire-mesh sensors and liquid film sensors based on the same signal acquisition method are very useful tools for an experimental characterization of the coolant flow in fuel rod bundles. They can be applied to cross-mixing experiments in plain liquid flow and for two-phase flow tests with flow patterns ranging from bubbly to annular flow. For the case of an annular flow, it was shown that the sensor data is very sensitive to the effect of the spacer geometry. Spacer studies on the 4 x 4 bundle SUBFLOW for under single phase and low void conditions are in preparation. The experimental data can therefore be used not only for code validation purposes, but the experimental techniques can be considered a valuable tool for the support of the optimization of fuel rod spacers. First steps were made towards a dense fuel rod lattice. The electrical liquid film thickness sensors were applied to a two-phase flow in a narrow gap.

In the present paper, only non-pressurized, adiabatic fluid dynamic experiments are reported. Nonetheless, the variation of the density of the gaseous phase in the tests on dynamic liquid films

can provide information on the sensibility of the film thickness and the wavy structures from the gas density, which is important for the transferability of the results to the conditions of the real reactor.

The theoretical modeling is on the way to reach a degree of maturity which allows for applying it to practical tasks. The presented method to predict the influence of spacers on the distribution of the liquid film thickness distribution, despite of the still existing uncertainties, is able to provide first estimates of the spacer effect and in this way support the search for an optimal geometry. In one hand, the strong approximations taken lead to the need of fitting model parameters (e.g. virtual liquid viscosity in the film, turbulent dispersion coefficient) to experiments, but on the other hand lead to a very fast-running numerical simulation, which can be used for scoping studies of a large variety of geometries.

LES is a very promising candidate for a fundamental modeling of the coolant flow in fuel rod bundles, though the numerical efforts are comparatively very high. First significant progress is reported concerning the single-phase cross-mixing between sub-channels, where the agreement with the experiment is very good. Two-phase flow modeling based on a coupling of LES and a surface tracking technique still require a continuation of intensive development, and, of course, the availability of very large computational power.

7. Symbols

Symbols	Unit	Description
D	m^2/s	Dispersion coefficient
J	m/s	Volume flow density, superficial velocity
S	m	Thickness
W	m	Width
В	_	Gas volume flow ratio

8. Acknowledgements

The article is summarizing the work of master and PhD students as well as postdocs from ETH Zurich, as well as contributions from researchers form the Paul Scherrer Institute. I would like to express my deep gratitude to all those who is standing behind the experimental and theoretical results: Arto Ylönen (SUBFLOW experiments), Manuel Damsohn (CALVIN experiments, liquid film modeling), Anders Kaestner, John Kickhofel, Eberhard Lehmann, Robert Zboray (Neutron Tomography), Daisuke Ito (bubbly flows in narrow gaps), Florian Reiterer, Bojan Niceno, Yohei Sato (LES modeling).

9. References

- [1] Johnson, I. D., 1987: Method and Apparatus for Measuring Water in Crude Oil, United States Patent, No 4,644,263, Date of Patent: Feb. 17, 1987.
- [2] Reinecke, N., Petritsch, G., Boddem, M., Mewes, D., 1998: Tomographic Imaging of the Phase Distribution in Two-phase Slug Flow, Int. J. Multiphase Flow 24 (1998)4, 617-634.
- [3] H.-M. Prasser, A. Bottger, J. Zschau, A new electrode-mesh tomograph for gas-liquid flow", Flow Meas. and Instr., 9, pp.111-119 (1998).

- [4] Teletronic GmbH: http://www.teletronic.net/
- [5] H.-M. Prasser, M. Beyer, A. Böttger, H. Carl, D. Lucas, A. Schaffrath, P. Schütz, F.-P. Weiß, J. Zschau, Influence of the pipe diameter on the structure of the gas-liquid interface in a vertical two-phase pipe flow, Nuclear Technology 152(2005) Oct, 3-22.
- [6] H.-M. Prasser, M. Beyer, H. Carl, S. Gregor, D. Lucas, H. Pietruske, P. Schütz, F.-P. Weiss, Evolution of the structure of a gas—liquid two-phase flow in a large vertical pipe, Nuclear Engineering and Design 237 (2007) 1848-1861.
- [7] H.-M. Prasser, M. Beyer, T. Frank, S. Al Issa, H. Carl, H. Pietruske, P. Schütz, Gas-liquid flow around an obstacle in a vertical pipe. Nuclear Engineering and Design 238 (2008) 1802–1819.
- [8] H. Pietruske, H.-M. Horst-Michael Prasser, Wire-mesh sensors for high-resolving two-phase flow studies at high pressures and temperatures. Flow Measurement and Instrumentation 18 (2007) 87–94.
- [9] H.-M. Prasser, G. Grunwald, T. Höhne, S. Kliem, U. Rohde, F.-P. Weiss, Coolant mixing in a PWR deboration transients, steam line breaks and emergency core cooling injection experiments and analyses, Nuclear Technology 143(2003), 37-56.
- [10] C. Walker, M. Simiano, R. Zboray, H.-M. Prasser, Investigations on mixing phenomena in single-phase flow in a T-junction geometry, Nucl. Eng. Des., 239(1), pp. 116-126 (2009).
- [11] S. Kliem, T. Sühnel, U. Rohde, T. Höhne, H.-M. Prasser, F.-P. Weiss, Experiments at the mixing test facility ROCOM for benchmarking of CFD codes. Nuclear Engineering and Design 238 (2008) 566–576.
- [12] S. Kliem, H.-M. Prasser, T. Sühnel, F.-P. Weiss, A. Hansen: Experimental determination of the boron concentration distribution in the primary circuit of a PWR after a postulated cold leg small break loss-of-coolant-accident with cold leg safety injection. Nuclear Engineering and Design 238 (2008) 1788–1801.
- [13] M. Damsohn, H.-M. Prasser, High-speed liquid film sensor for two-phase flows with high spatial resolution based on electrical conductance, Flow Measurement and Instrumentation 20 (2009) 1-14.
- [14] K. Mishima, T. Hibiki, Y. Saito, H. Nakamura, M. Matsubayashi, The review of the application of neutron radiography to thermal hydraulic research. Nucl. Inst. Meth. A 424 (1999) 66-72.
- [15] K. Mishima, T. Hibiki, Development of high-frame-rate neutron radiography and quantitative measurement method for multiphase flow research, Nuclear Engineering and Design 184(1998) 183–201.
- [16] Y. Saito, K. Mishima, Y. Tobita, T. Suzuki and M. Matsubayashi, Visualization and Measurements of Velocity Fields and Void Fraction in Gas-liquid Metal Two-Phase Flow by Neutron Radiography, 4th International Conference on Multiphase Flow, May 27 June 1, 2001, New Orleans, USA, paper 866.
- [17] http://www.psi.ch/science/large-scale-facilities

- [18] E.H. Lehmann, L. Josic, G. Frei, Material Research with Neutron Imaging Methods at SINQ. Neutron News, 20(2009 3, 20-23.
- [19] E.H. Lehmann, G. Frei, G. Kuhne, P. Boillat, The micro-setup for neutron imaging: A major step forward to improve the spatial resolution. Nucl. Inst. Meth. A, 576 (2007), 389-896.
- [20] N. Takenaka, H. Asano, T. Fujii, M. Matsubayasi, Three-dimensional visualization of void fraction distribution in steady teo-phase flow by thermal neutron radiography. Nuclear Engineering and Design, 184(1998) 203–212.
- [21] N. Takenaka, H. Asano, Quantitative CT-reconstruction of void fraction distributions in two-phase flow by neutron radiography. Nucl. Inst. Meth. A, 542 (2005) 387–391.
- [22] N. Takenaka H. Asano T. Fujii, M. Mizubata, K. Yoshii, Application of fast neutron radiography to three-dimesnional visualization of steady two-phase flow in a rod bundle. Nucl. Inst. Meth. A 424(1999) 73-76.
- [23] E.C. Lim, C.M. Sim, J.E. Cha, Y.S. Choi, N. Takenaka, Y. Saito, B.J. Jun, Measurement of the void fraction in a channel simulating the HANARO fuel assembly using neutron radiography. Nucl. Inst. Meth. A, 542 (2005) 181-186.
- [24] M. Kureta, Development of a neutron radiography three-dimensional computed tomography system for void fraction measurement of boiling flow in tight lattice rod bundles. Journal of Power and Energy Systems, 1(3) (2007) 211-224.
- [25] M. Kureta, Experimental study of three-dimensional void fraction distribution in heated tight-lattice rod bundles using three-dimensional neutron tomography. Journal of Power and Energy Systems, 1(3) (2007), 225-238.
- [26] M. Kureta, H. Tamai, H. Yoshida, A. Ohnuki, H. Akimoto, Development of design technology on thermal-hydraulic performance in tight-lattice rod bundles: V-Estimation of void fraction. Journal of Power and Energy Systems, 2(1) (2008), 271-282. [1] R.H. Brown, "A method to make reference to literature", Journal of Citation, Vol. 11, No. 2, 1988, pp. 195-204.
- [27] A. Ylönen, W.-M. Bissels, H.-M. Prasser, Single-phase cross-mixing measurements in a 4×4 rod bundle, Nuclear Engineering and Design 241 (2011), 2484-2493.
- [28] A. Ylönen, H.-M. Prasser, TWO-PHASE FLOW AND CROSS-MIXING MEASUREMENTS IN A ROD BUNDLE, The 14th International Topical Meeting on Nuclear Reactor Thermalhydraulics, NURETH-14 (accepted), 2011, paper 068.
- [29] B. Niceno, Y. Sato, A. Badillo, And M. Andreani, Multi-scale modeling and analysis of convective boiling: towards the prediction of CHF in rod bundles, Nuclear Engineering and Technology, 42(2010)6, 620-635.
- [30] F. Reiterer, Simulation of Single-Phase Mixing in Fuel Rod-Bundles Using an Immersed Boundary Method, Master Thesis M.Sc. ETH Zurich EPF Lausanne in Nuclear Engineering, Mai 2011.
- [31] A. Tomiyama, H. Tamai, I. Zun, S. Hosokawa, Transverse migration of single bubbles in simple shear flows, Chemical Engineering Science 57 (2002) 1849–1858.

- [32] H.-M. Prasser, D. Scholz, C. Zippe, Bubble size measurement using wire-mesh sensors, Flow Measurement and Instrumentation 12/4 (2001) 299-312.
- [33] H.-M. Prasser, E. Krepper, D. Lucas, Evolution of the two-phase flow in a vertical tube decomposition of gas fraction profiles according to bubble size classes using wire-mesh sensors, International Journal of Thermal Sciences, 41 (2002) 17-28.
- [34] Brereton, G. and D. Korotney, Coaxial and oblique coalescence of two rising bubbles. In Dynamics of Bubbles and Vortics Near a Free Surface. Vol. 119. 1991, New York: ASME.
- [35] M. Damsohn, H.-M. Prasser, Experimental studies of the effect of functional spacers to annular flow in subchannels of a BWR fuel element, Nuclear Engineering and Design 240 (2010) 3126-3144.
- [36] M. Damsohn, Liquid films and droplet deposition in a BWR fuel element, PhD thesis No. 19527, ETH ZURICH, 2011.
- [37] J. L. Kickhofel, R. Zboray, M. Damsohn, A. Kaestner, E. H. Lehmann, H.-M. Prasser, Cold neutron tomography of annular coolant flow in a double subchannel model of a boiling water reactor, Nucl. Instr. and Meth. A (2011), in press.
- [38] R. Zboray, J. Kickhofel, M. Damsohn, H.-M. Prasser, Cold-neutron tomography of annular flow and functional spacer performance in a model of a boiling water reactor fuel rod bundle, Nucl. Eng. Des. (2011), in press.
- [39] M. Damsohn and H.-M. Prasser, Towards efficient modeling of time-averaged film thickness distribution downstream of BWR functional spacers: model proposal and experimental validation, NURETH-14, Toronto, Ontario, Canada, September 25-30, 2011, NURETH14-412.
- [40] Kishore, B. N. and S. Jayanti, 2004. A multidimensional model for annular gas-liquid flow. Chemical Engineering Science, 59, 17, 3577-3589.
- [41] Bai and Gosman, 1996. Mathematical modeling of wall films formed by impinging sprays. S.A.E. Transactions, 6, 782-796.
- [42] Tso, C. P. and S. Sugawara, 1990. Film thickness prediction in a horizontal annular two-phase flow. International Journal of Multiphase Flow, 16, 5, 867-884.
- [43] M. Damsohn, H.-M. Prasser, Droplet deposition measurement with high-speed camera and novel high-speed liquid film sensor with high spatial resolution, Nuclear Engineering and Design 241 (2011) 2494-2499.
- [44] D. Ito, M. Damsohn, H.-M. Prasser, M. Aritomi, Dynamic film thickness between bubbles and wall in a narrow channel, Experiments in Fluids, 2011, Online First, 1-13.